Kinetic modeling of CO_2 + CO hydrogenation to DME over a CuO-ZnO-ZrO_2@SAPO-11 core-shell catalyst

Ainara Ateka*, Miguel Sánchez-Contador, Ander Portillo, Javier Bilbao, Andres T. Aguayo

Department of Chemical Engineering, University of the Basque Country UPV/EHU, P.O. Box 644, 48080 Bilbao, Spain

*Corresponding author. *Tel.:* 34-94-6015361. *E-mail address*: ainara.ateka@ehu.eus

ABSTRACT

A kinetic model for the CO_2 + CO hydrogenation to dimethyl ether (DME) in a single step over an original core-shell structured CuO-ZnO-ZrO_2@SAPO-11 bifunctional catalyst (metallic in the core and acid in shell) has been established. The catalytic runs have been carried out in an isothermal fixed bed reactor under the following conditions: 250-320 ºC; 10-50 bar; space time, 1.25-15 $g_{cat}\cdot h\cdot mol_C^{-1}$; H_2/CO_x molar fraction in the feed, 2.5-4, and CO_2/CO_x, 0-1. The catalyst has a high activity and stability as a result of the separation of reactions in the two functions.The model describes the effect of the operating conditions (temperature, pressure and feed composition) over the evolution of product distribution with time on stream. For this, the individual reactions (CO_2 and CO hydrogenation to methanol, its dehydration to DME, the WGS reaction and the side reaction of hydrocarbons formation) are considered together with catalyst deactivation. Using the model, simulation studies allow for establishing suitable operating conditions (305 ºC,70 bar, CO_2/CO_x of 0.75 and H_2/CO_x of 3) to attain a good compromise between DME yield and CO_2 conversion, reaching a value of 23 % for both objectives.

KEYWORDS: Model; deactivation; core-shell; CO_2; valorization; dimethyl ether

GRAPHICAL ABSTRACT

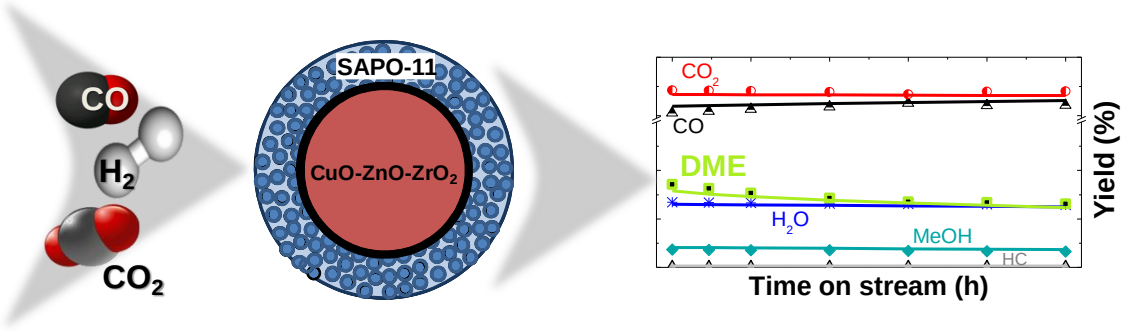

1. INTRODUCTION

The halt of climate change requires reducing the consumption of fossil sources and the implementation of new sustainable processes for the valorization of CO_2 and for the alternative production of fuels and energy vectors [1,2]. Among the catalytic processes under study for the conversion of CO_2, the direct synthesis of dimethyl ether (DME) receives great attention and has good prospects for its large-scale industrial implementation, due to the interest of DME economy and the capacity of the process to valorize CO_2 co-fed with synthesis gas.

DME is a good domestic and diesel engine fuel because its properties are similar to those of the Liquefied Petroleum Gases (LPG) and it has a high cetane number, which facilitates its storage and distribution [3,4]. Its utilization for power production in turbines is also interesting [5]. In addition, the viability of the selective conversion of DME into light olefins [6,7], aromatics or gasoline [8,9] is well established. Besides, DME has other applications, as for example, its use as refrigerant or green solvent [10,11], or in the enhanced oil recovery [12].

The synthesis of DME comprises the following reactions:

Methanol synthesis from CO: $CO + 2H_2 \leftrightarrow CH_3OH$ (1)

Methanol dehydration to DME: $2CH_3OH \leftrightarrow CH_3OCH_3 + H_2O$ (2)

Reverse water gas shift (rWGS): $CO_2 + H_2 \leftrightarrow CO + H_2O$ (3)

Besides, the direct hydrogenation of CO_2 to methanol (MeOH) also take place, and is described according to the following reaction:

$$CO_2 + 3H_2 \leftrightarrow CH_3OH + H_2O \quad (4)$$

Moreover, the undesired side reaction of paraffins formation may also takes place, giving way mainly to methane:

$$nCO + (2n+1)H_2 \leftrightarrow C_nH_{2n+2} + nH_2O \quad (n=1\text{-}3) \qquad (5)$$

The direct synthesis of DME is carried out with bifunctional catalysts under pressure and temperature conditions intermediate to those corresponding to the individual reactions of methanol synthesis (Eqs. 1 and 4) and its dehydration to DME (Eq. 2). Conceptually, the integration of the two reactions in a single reactor has lower equipment costs and also facilitates the displacement of the thermodynamic equilibrium of methanol synthesis reactions, since it is *in situ* dehydrated to DME. The thermodynamic advantages of direct synthesis of DME with respect to two-stage synthesis and to the synthesis of methanol have been compared in the literature [13,14]. Among the practical consequences of these advantages, the following are to be mentioned: i) the greater conversion of CO_2 when it is co-fed together with syngas, and; ii) the lower H_2/CO ratio required, which facilitates the valorization of the syngas derived from biomass and from different sources (coal, natural gas, biomass, plastics, tires). These advantages and the availability of natural gas and the important development of gasification and reforming technologies justify the attention received in the literature by the direct synthesis of DME [15,16]. This attention has focused mainly on the development of new catalysts [17] and new reactors [18]. The most studied reactors are fixed-bed reactors. Moradi et al. carried out a three dimensional dynamic CFD simulation for the direct DME production from CO and CO_2 hydrogenation in a fixed bed reactor. [19,20]. Slurry reactors have also been used for DME synthesis from CO hydrogenation. Papari et al. developed an axial dispersion mathematical model to simulate a slurry bubble column reactor for this reaction [21,22]. This model has been extended to other reactor types [23]. The isothermicity of the fluidized bed reactor is

interesting to control the temperature in different catalytic processes, in which the gas flow is considered with a two-phase model [24]. In this regard, Abashar et al. described a model to simulate a two-phase fluidized bed reactor for DME synthesis. [25].

Traditionally, in the bifunctional catalysts used in the direct synthesis of DME the metallic (for methanol synthesis) and acid (for its dehydration to DME) functions are integrated into the same particle by pelletization, in order to achieve the required mechanical strength for its use in the reactor and also to favor the synergy of the catalytic activity of the two functions. As acid function, HZSM-5 zeolite (less hydrophilic) has replaced the γ-Al_2O_3 initially used together with the CuO-ZnO metallic function (with different promoters). Despite the moderate-medium acidity of HZSM-5 zeolite, in order to limit the formation of hydrocarbons (coke precursors) in methanol dehydration, the incorporation of metals is used to passivate the strong acid sites [26]. This strategy and the partial dealumination are effective for minimizing side reactions activity and stabilizing zeolites [27].

However, the close contact of the metallic and acid sites also favors the synergy of the coke formation mechanisms in each type of sites and the migration of components, which causes the irreversible deactivation of these sites [28-30].

The use of catalyst particles with core-shell structure is an attractive initiative to preserve the properties of the metallic catalysts and attenuate their sintering [31-33], poisoning [34] or the formation of coke through side reactions [35]. In addition, the separation of the individual reactions in different regions of the catalyst particle improves the selectivity in complex reactions such as Fischer-Tropsch [36]. Thus, the direct synthesis of DME by CO and CO_2 hydrogenation has been studied in the literature, with core-shell catalysts of different composition such as Cu-ZnO-Al_2O_3@HZSM-5 [37-39], CuO-ZnO@HZSM-5 [40], Cr-ZnO@HZSM-5 [41],

$CuO\text{-}ZnO\text{-}Al_2O_3@SiO_2\text{-}Al_2O_3$ [42] or $Al_2O_3@Cu$ [43]. In previous works, the preparation and the advantages of a bifunctional $CuO\text{-}ZnO\text{-}ZrO_2$@SAPO-11 (CZZr@S-11) core-shell catalyst for the direct synthesis of DME have been studied, and its performance has been compared with that of a catalyst with conventional configuration (prepared by pelletization of the metallic and acid functions) [44]. Among these advantages, the greater activity and stability (lower deactivation) of the CZZr@S-11 catalyst are to be highlighted. The separation of methanol synthesis and dehydration reactions in two regions facilitates the separation of water from the first, favoring the activity of the catalyst for methanol synthesis, which explains the higher activity of the catalyst. The separation of the two reactions also prevents the deactivation phenomena previously stated [28-30]. Consequently, the CZZr@S-11 core-shell catalyst is very stable below 325 ºC, and only suffers a slow deactivation by coke [44,45].

The implementation of the CZZr@S-11 catalyst on a larger scale requires having a kinetic model suitable for the design of the reactor, which allows assessing the effects of the process conditions on products yields and distribution. Given the industrial relevance of the main reactions involved, the mechanisms and kinetic models for methanol synthesis [46-50]; its dehydration [51-54] and WGS reaction [55-59] are well established in the literature. However, these kinetic equations have been obtained under the suitable conditions (pressure, temperature) for each of these reactions and with a composition of the reaction medium that is also different from that in the direct synthesis of DME. It is also noteworthy that catalyst deactivation is not quantified. As to the direct synthesis of DME regards, kinetic models have been previously reported for different conventional bifunctional catalysts (hybrid) such as

$CuO-ZnO-Al_2O_3/\gamma-Al_2O_3$ [60] or CuO-ZnO-MnO/SAPO-18 [61], but no kinetic equation has been established for a catalyst with core-shell configuration.

In the present work, a kinetic model has been established for the direct synthesis of DME with the CZZr@S-11 core-shell catalyst, in a wide range of reaction conditions (temperature, pressure, space time, $CO_2/(CO+CO_2)$ and $H_2/(CO+CO_2)$ molar ratios in the feed).

2. EXPERIMENTAL

2.1. Catalyst preparation and characterization

The CZZr@S-11core-shell-like catalyst, has been prepared by physically coating the CZZr metallic function with the S-11 acid function, in a mass ratio of 1/2 as described in detail in previous works [44,45]. The good performance of the $CuO-ZnO-ZrO_2$ (CZZr) function and its adequate composition for the synthesis of methanol were studied in a previous work [62]. SAPO-11 (S-11) has a structure made up of elliptical one-dimensional channels of 0.4x0.6 nm. In addition, it has a high total acidity, but with sites of weak acid strength. These properties lead to high activity for the stage of methanol dehydration to DME, but a low activity for the side reactions of hydrocarbons and coke formation. This good behavior has been ascertained in a previous work [63]. As to the core-shell preparation methodology respects, over the CZZr cores (90-120 μm) the adhesion of the S-11 has been conducted by using a silica solution (Ludox TMA-34, Aldrich) as adhesive, following procedures described in the literature [64-66]. The resulting particles have been dried and calcined at 400 ºC for 2 h, and the strengthened core-shell particles sieved to 125-800 μm. For this purpose, the $CuO-Zn-ZrO_2$ metallic function was previously prepared following a conventional method of co-precipitation of the metallic nitrates in the desired proportions (Cu:Zn:Zr = 2:1:1) with

Na_2CO_3 and calcined at 300 ºC for 10 h [62]; and the SAPO-11 crystallized (at 195 ºC for 24 h) in a Berghof Highpreactor BR-300 teflon coated autoclave from H_3PO_4 (Merk), Ludox AS-40 (Aldrich) and Disperal (Sasol) and di-propylamine (Aldrich) as organic template, and calcined at 575 ºC for 8 h [63].

The textural properties of the catalyst were characterized by N_2 adsorption–desorption at -196 ºC, using a Micromeritics ASAP 2010. Prior to the measurements, the sample was degassed at 150 ºC for 8 h as for removing possible impurities. Using the Brunauer-Emmett-Teller equation, the specific surface area was determined from the isotherm; and using the BJH method in the adsorption branch of the isotherm, the total pore volume and the micropore volume were determined. The metallic content (Cu:Zn:Zr) has been analyzed by ICP-OES (Inductively Coupled Plasma Optical Emission Spectrometry) in a Perkin Elmer Optima 8300 apparatus; whereas the metallic properties (Cu surface area and dispersion) were determined by selective N_2O chemisorption in a Micromeritics Autochem 2920 Apparatus coupled on-line to a Mass Spectrometer (Pfeiffer-Vacuum Omnistar). The acidity and acid strength have been measured by combining thermogravimetry and calorimetry of NH_3 adsorption at 150 ºC and subsequent temperature programmed desorption (at 5 ºC·min^{-1} rate up to 550 ºC) using a Setaram TG-DSC 111 equipment coupled to a Balzers Instruments Thermostar Mass Spectrometer. Table 1 summarizes the most relevant properties of the catalyst. However, further analyzes such as, Scanning Electron Spectroscopy to assess the internal structure of the catalyst; Energy Dispersive X-ray spectroscopy to analyze each section of the catalyst; XRD to study the structural properties, and; Temperature Programmed Reduction (TPR) to ensure the complete reduction of CuO to Cu^0 [62] have been carried out. For the characterization of the coke content deposited on the used catalysts, the CO_2 signal resulting from Temperature Programmed Oxidation analyzes

(conducted in a TA Instruments TGA Q5000 apparatus) has been registered in a Mass Spectrometer (Balzers Instruments). For the quantitative measurement of CO_2 in the combustion gases, $CaCO_3$ has been added to each sample as internal standard (decomposes at higher temperature than the combustion compounds) [67].

Table 1. Textural, metallic and acid properties of the CZZr@S-11 catalyst.

Textural properties		
S_{BET} ($m^2 \cdot g^{-1}$)	V_m ($cm^3 \cdot g^{-1}$)	V_p ($cm^3 \cdot g^{-1}$)
123	0.031	0.300
Metallic properties		
S_{Cu} ($m^2 \cdot g_{Cu}^{-1}$)	S_{Cu} ($m^2 \cdot g_{cat}^{-1}$)	Dispersion (%)
33.3	3.9	5.1
Acid properties		
Acid strength ($kJ \cdot mol_{NH3}^{-1}$)	Total acidity ($mmol_{NH3} \cdot g_{cat}^{-1}$)	
85	0.186	

2.2. Reaction equipment and catalytic runs

The reaction runs have been carried out in an automated reaction equipment (Microactivity reference, PID Eng. Tech. Micromeritics) provided with a high pressure packed bed stainless steel 316 reactor, of 9 mm of internal diameter and 100 mm of effective length. The used equipment is capable for operating up to 100 atm and 700 ºC, and has been described in detail in previous works [45,68]. In order to ascertain that the kinetics is not affected by the limitations of the stages of diffusion inside and outside the particles, theoretical and experimental criteria of the literature have been adopted [69]. Thus, the absence of diffusion limitations for catalyst particles in the 0.1-0.5 mm range and feeding a total gas flowrate of 60 $cm^3 \cdot min^{-1}$ to the reactor has been determined. Consequently, those have been selected as run conditions.

For each run, the catalyst was diluted with an inert solid (SiC of average particle size of 0.035 mm) to ensure isothermal conditions and attain a constant bed height in all the runs. Prior to the reactions, the catalyst was subjected to a reduction treatment with diluted H_2 (at 250 ºC) for the complete reduction of the Cu to Cu^0, active species. The experimental conditions used for the direct synthesis of DME from CO_2 and CO were: 250-325 ºC; 10-50 bar, space-time, 1.25-15 $g \cdot h \cdot mol_C^{-1}$; CO_2/CO_x molar ratio, 0-1; and H_2/CO_x molar ratio, 2.5-4; time on stream, up to 48 h.

The reaction products were analyzed in a gas-chromatograph (Varian CP-4900) coupled on line to the reaction equipment. The chromatograph is provided with different modules allowing to identify the following compounds: i) Porapak Q for analyzing C_1-C_3 hydrocarbons, CO_2, H_2O, methanol (MeOH) and DME; ii) MS-5 molecular sieve for analyzing H_2 and CO.

3. RESULTS AND DISCUSSION

The calculation steps for establishing a kinetic equation capable for quantifying products distribution and yields evolution with time on stream, thus, considering catalyst deactivation are described below. Ideal plug flow has been considered in the packed bed reactor, without radial gradients of concentration and temperature (ensured experimentally to be less than 1 ºC).

3.1. Methodology for the kinetic study

Toch et al. [70] have explained the main steps of the modeling methodology used in catalytic processes with complex reaction schemes. More recently, Cordero-Lanzac et al. [71] have established a data analysis methodology for determining the kinetic

parameters of the different stages involved in the reaction scheme together with the deactivation kinetics. In this case, first, the kinetic parameters have been calculated at zero time on stream and subsequently, in a second calculation step, the deactivation kinetic equation has been established by minimizing a second objective function, that includes a term related to the lack of fit at zero time on stream and another term related to the deactivation kinetics (as detailed in the Supporting information Section).

The first step of the modeling consisted of determining the parameters of the kinetic equations proposed in the reaction stages (Eqs. (1)-(5)). For this purpose, the experimental results of the concentration of each component *i* at zero time on stream have been fitted to the value determined by integrating the corresponding conservation equation:

$$r_{i,0} = \frac{dy_i}{d\left(W/F_0\right)} \tag{6}$$

Where $r_{i,0}$ is the formation rate of component *i* at zero time on stream ($mol_C \cdot g^{-1} \cdot h^{-1}$); y_i is the molar fraction of component *i* (in equivalent C units); W is the mass of catalyst (g); and F_0, the molar flow rate of C fed as CO and CO_2 ($mol_C \cdot h^{-1}$).

The reactions have been considered to be elementary, that is:

$$r_{i,0} = \sum_{j=1}^{n_j} (\upsilon_i)_j \, r_{j,0} \tag{7}$$

where $(\upsilon_i)_j$ is the stoichiometric coefficient of component *i* in the *j* step of the kinetic scheme (corresponding to Eqs. (1)-(5)); $r_{i,0}$ is the formation rate of *i* at zero time on stream; $r_{j,0}$ the rate of j reaction step at zero time on stream and n_j the number of equations involved in the reaction scheme. Note that for Eq. (5), all the resulting

hydrocarbons (C_1-C_3) have been grouped into a lump, since the amount produced is very low, and methane is predominant.

For considering catalyst deactivation, an activity term (a) has been defined as the ratio between the reaction rates at time *t* and at zero time on stream as:

$$a = \frac{r_j}{r_{j,0}} \tag{8}$$

Accordingly, the formation rate of component *i*, at a certain t time is given by:

$$r_i = \frac{dy_i}{dt} = (r_{i,0})\, a = \sum_{j=1}^{n_j} (\upsilon_i)_j r_{j,0} a \tag{9}$$

The methodology used for determining the kinetic parameters and for assessing the significance and validity of the models, have been described in detail in the Supporting Information, and are based on previous studies of the authors already reported in the literature [60,61].

3.2. Proposed kinetic models

The study has been conducted by fitting the experimental results to progressively more complex models, in which terms considering the attenuation of the reaction (and deactivation) rates by adsorption of H_2O and/or CO_2 on the active sites have been included. The first and most simple model (Model 1) considers elementary reactions for the rates of methanol formation from CO (Eq. (10)), the dehydration of this to DME (Eq. (11), the WGS reaction (Eq. (12) and the formation of hydrocarbons (being independent of reaction conditions) (Eq. (13)).

$$r_{MeOH} = k_1 \left[f_{H_2}^2 f_{CO} - \frac{f_{CH_3OH}}{K_1} \right] \tag{10}$$

$$r_{DME} = k_2\left[f_{CH_3OH}^2 - \frac{f_{CH_3OCH_3} f_{H_2O}}{K_2}\right] \quad (11)$$

$$r_{WGS} = k_3\left[f_{H_2O} f_{CO} - \frac{f_{CO_2} f_{H_2}}{K_3}\right] \quad (12)$$

$$r_{HC} = \beta \quad (13)$$

The next Model 2, modifies Model 1 considering the synthesis of methanol also from CO_2 hydrogenation (reaction in Eq. (4)). Thus, methanol formation kinetic is given by:

$$r_{MeOH} = k_1\left[f_{H_2}^2 f_{CO} - \frac{f_{CH_3OH}}{K_1}\right] + k_4\left[f_{H_2}^3 f_{CO_2} - \frac{f_{CH_3OH} f_{H_2O}}{K_4}\right] \quad (14)$$

Model 3, unlike the previous models in which the formation of hydrocarbons has been considered to be independent of temperature, assess different pathways for the formation of hydrocarbons. The Model 3A considers that these compounds are formed through thermal routes (DME decomposition), and so, its formation rate is linearly dependent on temperature (Eq. (15)). Model 3B considers that hydrocarbons formation occurs through catalytic routes being CO the reactant (methanation and Fischer Tropsh synthesis) (Eq. (16)); whereas Model 3C considers both the thermal and catalytic routes at a time (Eq. (14)). However, it should be noted that the yield of hydrocarbons (C_1-C_3 paraffins) is below 0.2 % in most cases, and does not surpass 1 % in any case, and therefore, the relevance of considering these alternatives will presumably be low.

$$r_{HC} = [\beta_1 + \beta_2(T)] \quad (15)$$

$$r_{HC} = \left[\beta_1 + k_5\left(f_{H_2}^3 f_{CO} - \frac{f_{HC} f_{H_2O}}{K_5}\right)\right] \quad (16)$$

$$r_{HC} = \left[\beta_1 + \beta_2(T) + k_5 \left(f_{H_2}^3 f_{CO} - \frac{f_{HC} f_{H_2O}}{K_5} \right) \right] \quad (17)$$

It must be stated that Model 3 does not improve the fitting acquired with Model 2 (as shown in the subsequent Section 3.3). Consequently, the subsequent models propose improvements using Model 2 as a basis. Thus, Model 4, includes the attenuating effect of H_2O adsorption on the active sites. This feature is characteristic of acid catalysts, [72,73], however, it has also been observed in the activity of the metallic function for the synthesis of methanol [30,74,75]. Model 4A considers this effect exclusively on the reactions of methanol synthesis (Eq. (18)). Model 4B considers the effect of H_2O adsorption on the reaction of methanol dehydration to DME (Eq. (19), 4C on the WGS reaction (Eq. (20)); and 4D on the hydrocarbons formation reaction (Eq. (21)). The effect has been quantified using a θ_{H2O} term in the corresponding kinetic equation:

$$r_{MeOH} = \left[k_1 \left[f_{H_2}^2 f_{CO} - \frac{f_{CH_3OH}}{K_1} \right] + k_4 \left[f_{H_2}^3 f_{CO_2} - \frac{f_{CH_3OH} f_{H_2O}}{K_4} \right] \right] \theta_{H_2O} \quad \text{(model 4A)} \quad (18)$$

$$r_{DME} = k_2 \left[f_{CH_3OH}^2 - \frac{f_{CH_3OCH_3} f_{H_2O}}{K_2} \right] \theta_{H_2O} \quad \text{(model 4B)} \quad (19)$$

$$r_{WGS} = k_3 \left[f_{H_2O} f_{CO} - \frac{f_{CO_2} f_{H_2}}{K_3} \right] \theta_{H_2O} \quad \text{(model 4C)} \quad (20)$$

$$r_{HC} = \beta \theta_{H_2O} \quad \text{(model 4D)} \quad (21)$$

where term θ_{H_2O} is dependent on the concentration of H_2O according to the following expression:

$$\theta_{H_2O} = \frac{1}{1 + + f_{H_2O} \cdot K_{ads,H_2O}} \quad (22)$$

the term $K_{ads,H2O}$ in Eq. (22) is related to the H_2O adsorption equilibrium constant.

Model 5 is based on model 4A, and apart from the influence of H_2O adsorption, includes that of the adsorption of CO_2 on the metallic sites with a θ_{H_2O,CO_2} term. In this case three alternatives have been proposed: i) considering the attenuating effect on the methanol synthesis reaction rates, model 5A (Eq. (23)); ii) on the WGS reaction, 5B (Eq. (24)), and; iii) on the hydrocarbons synthesis reaction, 5C (Eq. (25)).

$$r_{MeOH} = \left[k_1 \left[f_{H_2}^2 f_{CO} - \frac{f_{CH_3OH}}{K_1} \right] + k_4 \left[f_{H_2}^3 f_{CO_2} - \frac{f_{CH_3OH} f_{H_2O}}{K_4} \right] \right] \theta_{H_2O,CO_2} \quad \text{(model 5A)} \quad (23)$$

$$r_{WGS} = k_3 \left[f_{H_2O} f_{CO} - \frac{f_{CO_2} f_{H_2}}{K_3} \right] \theta_{CO_2} \quad \text{(model 5B)} \quad (24)$$

$$r_{HC} = \beta \theta_{CO_2} \quad \text{(model 5C)} \quad (25)$$

where term θ_{H_2O,CO_2} is: $\theta_{H_2O,CO_2} = \dfrac{1}{1 + f_{H_2O} \cdot K_{ads,H_2O} + f_{CO_2} \cdot K_{ads,CO_2}}$ (26)

and term θ_{CO_2} is: $\theta_{CO_2} = \dfrac{1}{1 + + f_{CO_2} \cdot K_{ads,CO_2}}$ (27)

being K_{ads,CO_2} the CO_2 adsorption equilibrium constant

Note that considering the terms of H_2O and CO_2 adsorption gives to Eqs. (23)-(25) the characteristic configuration of Langmuir-Hinshelwood (LH) kinetic expressions.

3.2.1. Deactivation kinetics

Preliminary TPO analyzes of the used catalysts [44,45] have allowed distinguishing two different mechanisms for coke deposition; i) a fast deposition mainly over the metallic function as a consequence of the degradation to coke of the methoxy and other reaction intermediates involved in the methanol formation from CO and CO_2, and; ii) a slower

and progressive coke deposition on the acid sites, which requires an induction period, and has been related to the routes of the hydrocarbon pool mechanism, side products also containing methoxy ions (produced from the methanol and DME adsorbed on the sites of the acid function) as intermediates. These mechanisms of coke formation are well established for the MTO (methanol to olefins) and DTO (DME to olefins) processes [76]. However, the high H_2 pressure in the studied conditions and the limited acid strength of the sites of the SAPO-11 in the catalyst are key features to attenuate the formation of coke. Giving the complexity of considering both routes, due to their different kinetics and bearing in mind that the first one only occurs during the first hour of reaction, special attention has been paid to the second route as this cause of deactivation progresses slowly with time on stream. Consequently, a deactivation kinetic equation has been established dependent on the concentration of the oxygenates (methanol and DME) in the reaction medium, due to its role in the generation of methoxy ions and subsequent formation of hydrocarbons precursors of coke [77,63]:

$$-\frac{da}{dt} = k_d\left(f_{MeOH} + f_{DME}\right)\theta_d \cdot a \qquad (28)$$

where k_d is the kinetic constant for deactivation.

In Eq. (28) a term θ_d has been considered for quantifying the attenuating effect of H_2O and CO_2 concentrations on the deposition of coke due to the limitation of the methoxy ions formation [77] and to the competition of these components with coke precursor hydrocarbons for their adsorption on the active sites (both on metallic and on acid sites). As mentioned, term θ_d gathers the attenuating effect of H_2O and CO_2 adsorption; anyhow, different expressions have been used in the kinetic models previously described. Thus, in Models 1-3 this effect has not been considered, and therefore, $\theta_d = 1$

has been established in Eq. (28). In Models 4 and 5 term θ_d has been considered according to the expressions described in Eqs. (29) and (30), respectively.

$$\theta_d = \frac{1}{1 + f_{H_2O} \cdot K^d_{ads,H_2O}} \qquad \text{(model 4)} \qquad (29)$$

$$\theta_d = \frac{1}{1 + f_{H_2O} \cdot K^d_{ads,H_2O} + f_{CO_2} \cdot K^d_{ads,CO_2}} \qquad \text{(model 5)} \qquad (30)$$

where K^d_{ads,H_2O} and K^d_{ads,CO_2} correspond to the adsorption constants of H_2O and CO_2 on the active sites involved in the deactivation by coke.

The equations considered in the different models have been summarized in Table 2.

Table 2. Studied kinetic models.

Model	**Equations**			
	$\mathbf{r_{MeOH}}$	$\mathbf{r_{DME}}$	$\mathbf{r_{WGS}}$	$\mathbf{r_{HC}}$
1	10	11	12	13
2	14	11	12	13
3A	14	11	12	15
3B	14	11	12	16
3C	14	11	12	17
4A	18	11	12	13
4B	14	19	12	13
4C	14	11	20	13
4D	14	11	12	21
5A	23	11	12	13
5B	18	11	24	13
5C	18	11	12	25

3.3. Discrimination of the kinetic models

Table 3 shows the main statistic parameters (sum of squares of the errors, SSE; degrees of freedom, ν; variances for the lack of fit, s^2) for each model and for the experimental results, whereas Table 4 gathers the values (Fischer distribution, F_{a-b}; and the critical value of Fisher distribution, $F_{1-\alpha}$) used for model discrimination (following the methodology described in the Supporting Information).

Table 3. Statistic parameters for each model, and for the experimental error.

Model	**SSE**	**ν**	**s^2**
1	3.36E-01	11251	$2.69 \cdot 10^{-1}$
2	3.36E-01	11246	$2.61 \cdot 10^{-4}$
3A	3.26E-01	1248	$2.61 \cdot 10^{-4}$
3B	3.26E-01	1247	$2.61 \cdot 10^{-4}$
3C	3.26E-01	1246	$2.61 \cdot 10^{-4}$
4A	3.16E-01	1242	$2.54 \cdot 10^{-4}$
4B	3.26E-01	1242	$2.63 \cdot 10^{-4}$
4C	3.26E-01	1242	$2.62 \cdot 10^{-4}$
4D	3.26E-01	1242	$2.62 \cdot 10^{-4}$
5A	2.52E-01	1238	$2.04 \cdot 10^{-4}$
5B	2.46E-01	1238	$1.99 \cdot 10^{-4}$
5C	2.59E-01	1238	$2.09 \cdot 10^{-4}$
Experimental	1.35E-01	581	$2.32 \cdot 10^{-4}$

Table 4. Statistic comparison for model discrimination.

F_{a-b}	F_{a-b}	$F_{1-\alpha}$	Improvement	Selected
F_{1-2}	18.67	3.001	Yes	2
F_{2-3A}	0.08	3.85	No	2
F_{2-3B}	0.67	3.00	No	2
F_{2-3C}	0.59	2.61	No	2
F_{2-4A}	5.70	2.02	Yes	4A
F_{2-4B}	0.08	2.02	No	2
F_{2-4C}	0.17	2.02	No	2
F_{2-4D}	0.20	2.02	No	2
F_{4A-5A}	78.08	2.38	Yes	5A
F_{4A-5B}	87.89	2.38	Yes	5B
F_{4A-5C}	69.09	2.38	Yes	5C

From the results in Tables 3 and 4, it is evident that considering successively methanol formation from CO_2 (Model 2), the attenuating effect of H_2O adsorption on the reaction and deactivation rates (Model 4) and the attenuating effect of CO_2 adsorption (Model 5) lead to relevant improvements on the fitting. On the other hand, given the low paraffin amount reported, using more kinetic parameters to analyze the origin of their formation is not worth it (Model 3). For comparing models 5A-5C, as they have equal degrees of freedom, a variance analysis has been carried out. Thus, that of lower variance has been selected (5B) since any of them implies an improvement over the other on fitting the experimental data. Finally it has been ascertained that the selected Model 5B satisfies the significance test in Eq. (S5) (Fs= 0.86), which means that the error associated to the lack of fit is lower than the experimental error, and so, that the model represents satisfactorily the experimental results.

The kinetic parameters of best fit (kinetic and adsorption constants at reference temperature, k* and K*, respectively, and activation energies and reaction heats, E and

ΔH, respectively) for the selected model (5B) have been listed in Table 5. It is noteworthy that the activation energy of methanol synthesis from CO (12.8 $kJ \cdot mol^{-1}$) is notably lower than that corresponding to its synthesis from CO_2 (84.5 $kJ \cdot mol^{-1}$). Furthermore, the kinetic constant at the reference temperature is greater for the synthesis from CO ($1.14\ 10^{-5}$ $mol_{MeOH} \cdot g^{-1} \cdot h^{-1} \cdot bar^{-3}$) than from CO_2 ($9.47\ 10^{-7}$ $mol_{MeOH} \cdot g^{-1} \cdot h^{-1} \cdot bar^{-4}$). These results, obtained by fitting the results to an empirical kinetic model, are consistent with the molecular simulation results of the DME synthesis by Qin et al. [78]. These authors determined by density functional theory (DFT) that methanol synthesis mechanism takes place through formate ions, with a lower energy barrier for the synthesis from CO than from CO_2. Consequently, they consider in their intrinsic reaction model that r-WGS (Eq. (3)) is key for the synthesis of methanol. In Table 5, the value of the kinetic constant at the reference temperature of methanol dehydration is very high (25.6 $mol_{DME} \cdot g^{-1} \cdot h^{-1} \cdot bar^{-2}$), which is also in accordance with the consideration of Qin et al. that the stage of methanol synthesis is slower than that of methanol dehydration and conditions the hydrogenation of CO_2 to DME [78]. On the other hand, the reaction heats corresponding to the constants related to de adsorption of H_2O and CO_2 on the metallic and acid sites ($K_{ads,H2O}$ and $K_{ads,CO2}$) are small, as correspond to physical adsorption. An interpretation of the values of the adsorption heats of H_2O and CO_2 cannot be made for the constants that quantify deactivation due to their empirical meaning.

Table 5. Kinetic parameters for Model 5B considering deactivation.

Parameter	units	k* or K* (at 275 ºC)	E or ΔH ($kJ \cdot mol^{-1}$)
k_1	$(mol_{MeOH} \cdot g^{-1} \cdot h^{-1} \cdot bar^{-3})$	$1.14 \cdot 10^{-5}$	$1.28 \cdot 10^{1}$
k_2	$(mol_{DME} \cdot g^{-1} \cdot h^{-1} \cdot bar^{-2})$	$2.56 \cdot 10^{1}$	$2.07 \cdot 10^{2}$
k_3	$(mol \cdot g^{-1} \cdot h^{-1} \cdot bar^{-2})$	$4.63 \cdot 10^{1}$	$9.33 \cdot 10^{1}$
k_4	$(mol_{MeOH} \cdot g^{-1} \cdot h^{-1} \cdot bar^{-4})$	$9.47 \cdot 10^{-7}$	$8.45 \cdot 10^{1}$
k_5	$(mol_{HC} \cdot g^{-1} \cdot h^{-1})$	$1.30 \cdot 10^{-3}$	-
$K_{ads,H2O}$	(bar^{-1})	$3.17 \cdot 10^{0}$	$8.70 \cdot 10^{-2}$
$K_{ads,\ CO2}$	(bar^{-1})	$1.16 \cdot 10^{-1}$	$1.56 \cdot 10^{-1}$
k_d	$(h^{-1} \cdot bar^{-1})$	$1.31 \cdot 10^{-1}$	$5.73 \cdot 10^{0}$
$K_{ads,H2O,d}$	(bar^{-1})	$1.37 \cdot 10^{-2}$	$9.12 \cdot 10^{-1}$
$K_{ads,CO2,\ d}$	(bar^{-1})	$1.26 \cdot 10^{-2}$	$9.71 \cdot 10^{-1}$

In order to show visually the fitting of the tested models to the experimental data, further information of the fitting obtained with Models 1, 2, 4A and 5B can be found in the Supporting Information (Fig. S1) and in Fig. 1, where the fitting to all the components in the reaction medium is depicted. For this and subsequent figures product yield has been defined as:

$$Y_i = \frac{n_i \cdot F_i}{F_{COx}^0} \cdot 100 \qquad (31)$$

where n_i is the number of carbon atoms in a molecule of component *i*; F_i the molar flowrate of component *i* at the reactor outlet, and F_{COx}^0 the molar flowrate of carbon in the reactor inlet stream fed as CO and/or CO_2.

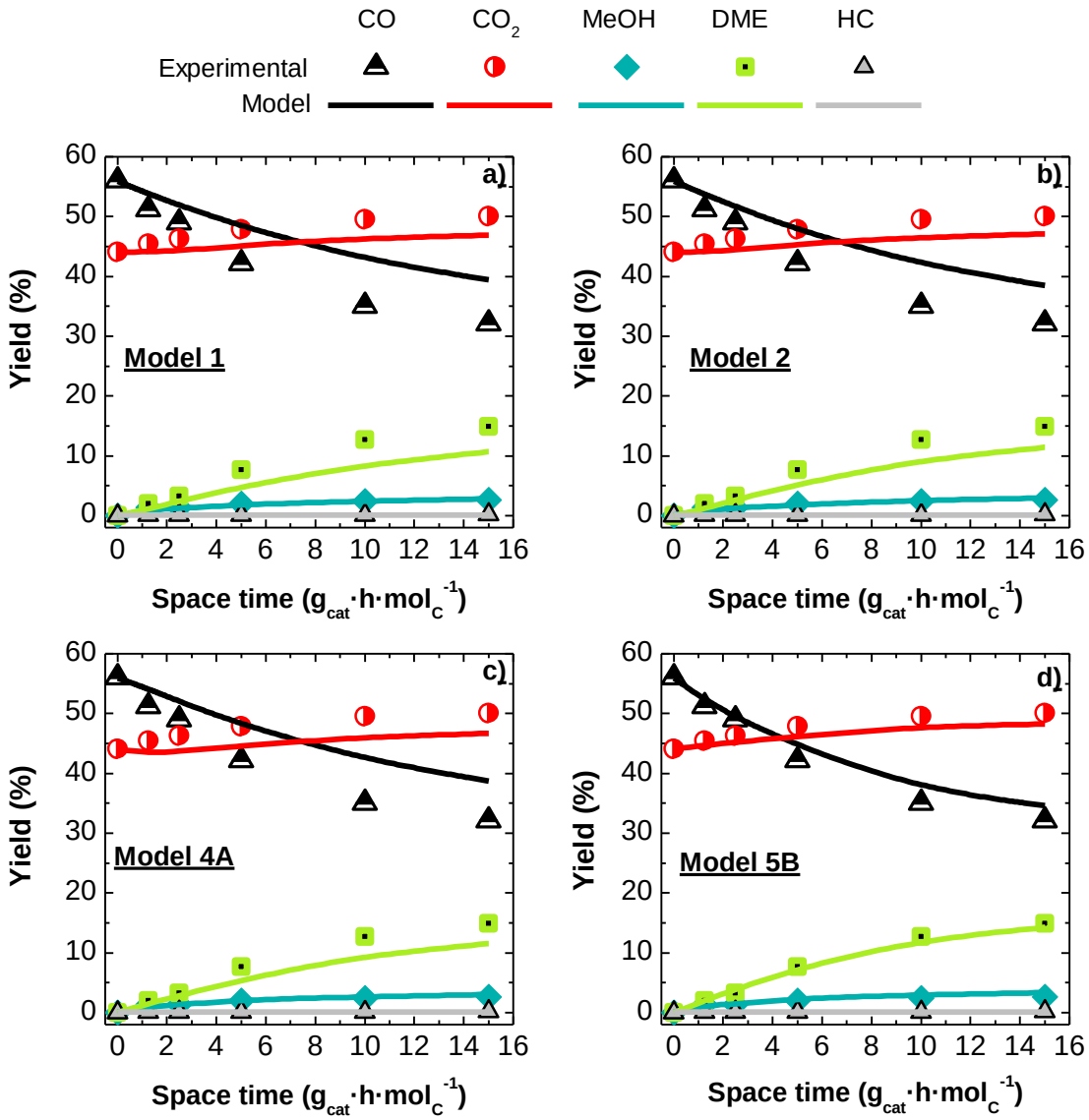

Figure 1. Fitting of models 1 (a), 2 (b), 4A (c) and 5B (d) to the experimental values of CO, CO_2, MeOH, DME and HC yields. Reaction conditions: 300 ºC, 30 bar, CO_2/CO_x= 0.5, H_2/CO_x= 3.

3.4. Fitting of the model to the experimental values

As an example, the fitting obtained with Model 5B at different operating conditions is depicted in Figure 2. The reaction conditions unless other indicated have been: 300 ºC; 30 bar; 5 $g_{cat}\cdot h\cdot mol_C^{-1}$; H_2/CO_x molar ratio in the feed of 3, CO_2/CO_x molar ratio in the feed of 0.5, and 5 h TOS. The study has been extended in the Supplementary Information Section, for other operating conditions, Figures S2-S6.

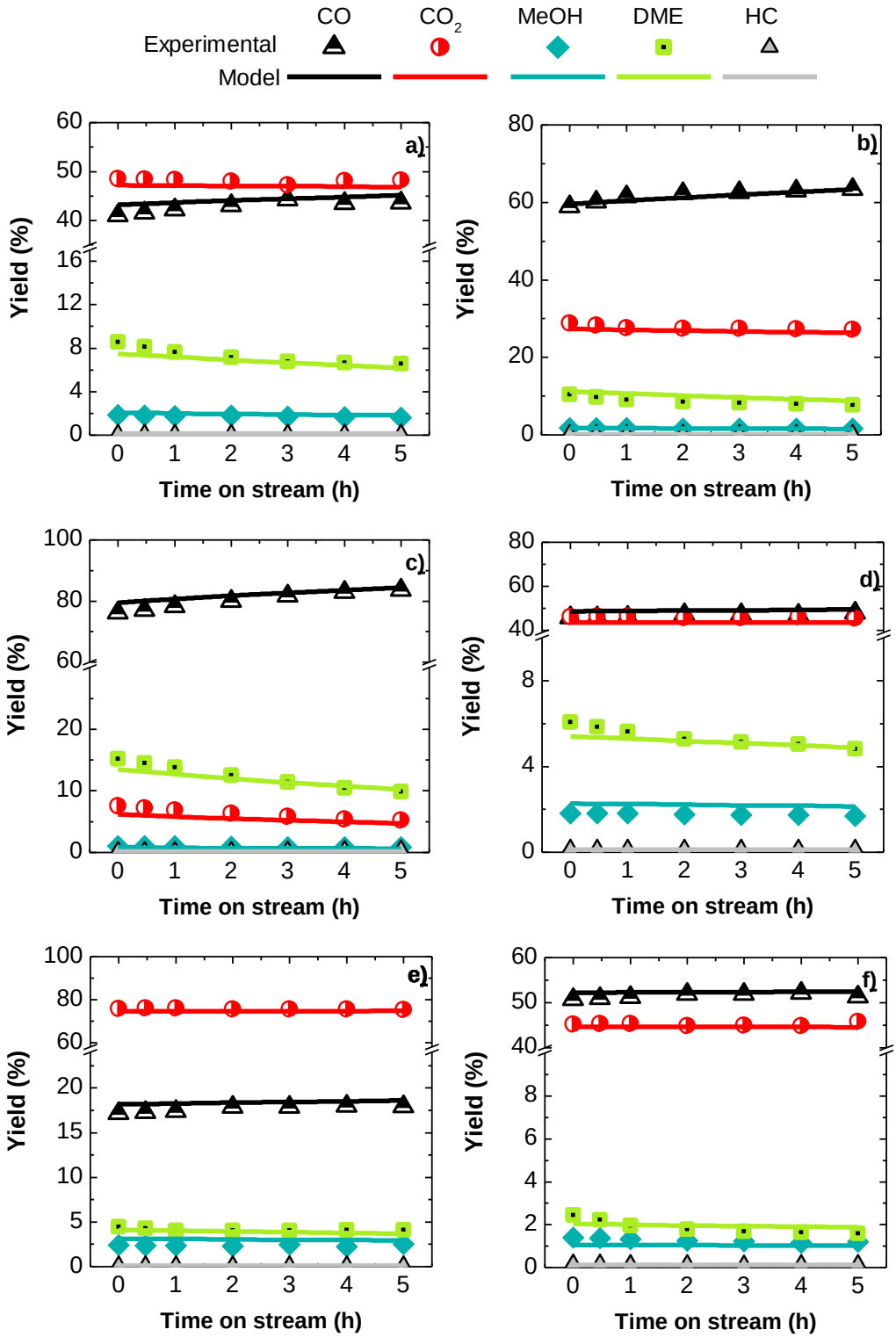

Figure 2. Fitting of the Model 5B to the experimental values of CO, CO_2, MeOH, DME and HC yields evolution with time on stream. Reaction conditions: a) 300 ºC; 30 bar; H_2/CO_x, 2.5; CO_2/CO_x, 0.5; space time, 5 $g_{cat}\cdot h\cdot mol_C^{-1}$; b) idem except H_2/CO_x, 4; c) idem except H_2/CO_x, 3 and CO_2/CO_x, 0 (syngas); d) idem except 325 ºC and CO_2/CO_x, 0.5; e) idem except 300 ºC and 40 bar; f) idem except 30 bar and space time 1.25 $g_{cat}\cdot h\cdot mol_C^{-1}$.

3.5. Reactor simulation

Once proved in the previous Section 3.4 that the proposed kinetic model is capable of describing the evolution of product distribution with TOS within the studied range of operating conditions, it has been used for simulating the operation in a fixed-bed isothermal reactor. Figure 3, shows the operating maps of DME yield for two different feeds; syngas ($CO+H_2$) and CO_2+H_2, as a function of reaction temperature and pressure. It can be observed that the CO_2 content in the feed has a remarkable influence on the yield of DME (Y_{DME}), decreasing from around 50 % for $CO+H_2$ feeds, to almost 10 % for CO_2+H_2 feeds at the most suitable conditions. For both feed compositions, Y_{DME} increases noteworthy upon increasing reaction pressure, and the optimum is located within the 280-300 ºC range, the lower limit corresponding to the maximum at higher pressure. Moradi et al. have studied by simulation of a fixed bed reactor the importance of pressure and temperature in the conversion of CO and selectivity of DME, obtaining as optimum a pressure of 50 bar [19,20]. The optimal temperature for these authors is 270 ºC in an adiabatic regime and 260 ºC in an isothermal regime. The differences in the results of these authors with those shown in Figure 3 for CO hydrogenation are moderate and are a consequence of the differences in the kinetic model (different catalyst). Furthermore, the results in Figure 3 correspond to an H_2/CO_x ratio of 3, and this ratio (suitable for CO and CO_2 hydrogenation) is of great relevance in the results [45], as also verified by Moradi et al. in the hydrogenation of CO [20].

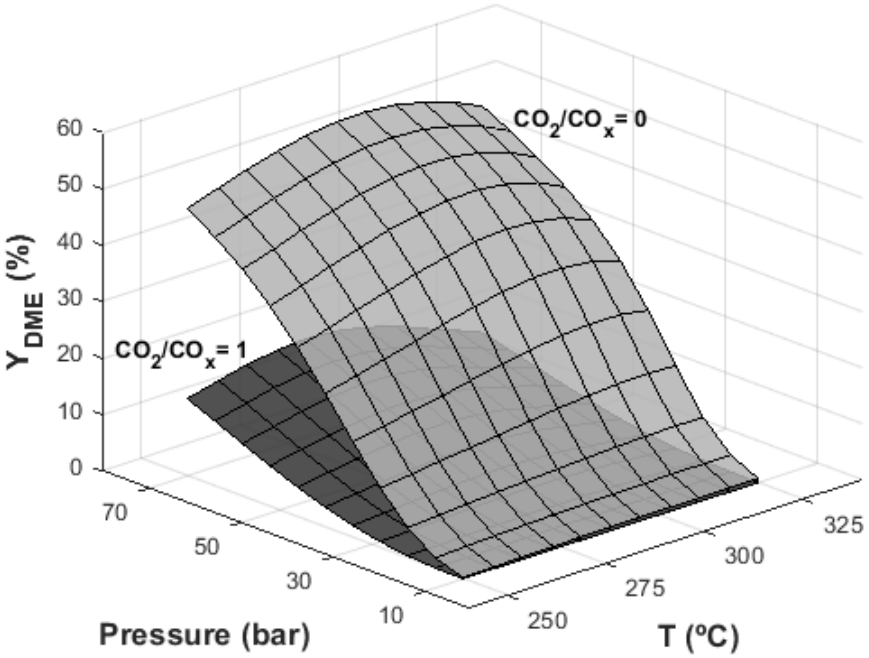

Figure 3. Evolution of DME yield with reaction temperature and pressure for CO_2/CO_x ratios in the feed of 0 (syngas, $CO+H_2$) and 1 (CO_2+H_2). Reaction conditions: $H_2+CO+CO_2$ feed; H_2/CO_x, 3; space time 5 $g_{cat}\cdot h\cdot mol_C^{-1}$; time on stream, 1 h.

As a favorable feature, the effect of feeding CO_2 on the attenuation of the deactivation is remarkable. Thus, after 1 h time on stream this deactivation is very slow when feeding CO_2, as it can be observed in Figures 2a, 2b, 2d, 2e and 1f, and in Figures S2-S6, when CO_2 is fed with a CO_2/CO_x ratio of 0.5 or above. This result is of great interest for the industrial viability of the process with this catalyst and is consistent with the deactivation kinetic equation, Eq. (30), which considers the competence of the adsorption of H_2O and CO_2 with coke precursors. Presumably, these precursors are hydrocarbons formed in the metallic sites by Fischer-Tropsch synthesis from CO, and in the acidic sites from the oxygenates (methanol and DME), by the generation of methoxy ions in this case, which are also active to generate hydrocarbons through the well established hydrocarbon pool mechanism [79]. In addition, the relationship between the

concentration of CO_2 and H_2O must be taken into account, since increasing the concentration of CO_2 in the feed will lead to an increase of the concentration of H_2O through the WGS reaction (Eq. (3)).

To illustrate the effect of co-feeding CO_2 on coke deposition, Figure 4 shows the TPO profiles for catalysts used in experiments without and with CO_2 in the feed, for the same reaction conditions. In these TPO runs, the fraction of the coke deposited on the metallic sites (CuO-ZnO-ZrO_2 function in the particle core) burns at low temperature (around 185 ºC) because its combustion is catalyzed by the metallic sites. The coke deposited on the acid sites of the SAPO-11 (in the shell of the particle) burns at higher temperature because its combustion is not catalyzed [45]. As it can be seen, co-feeding CO_2 attenuates the deposition of coke on the metallic sites and makes the deposition on the acid sites insignificant. This effect may be related to the higher H_2O content in the reaction medium, whose attenuation effect of coke formation has also been verified in other reactions, such as propane dehydrogenation [80] or vacuum gas oil (VGO) cracking [81].

It is also noteworthy that the deposition of coke when co-feeding CO_2 is lower with the core-shell catalyst than with the conventional structure catalyst (0.25 wt% vs 0.57 wt%, respectively [44]) which corroborates the lower synergy in the mechanisms of coke formation in the metallic and acid functions.

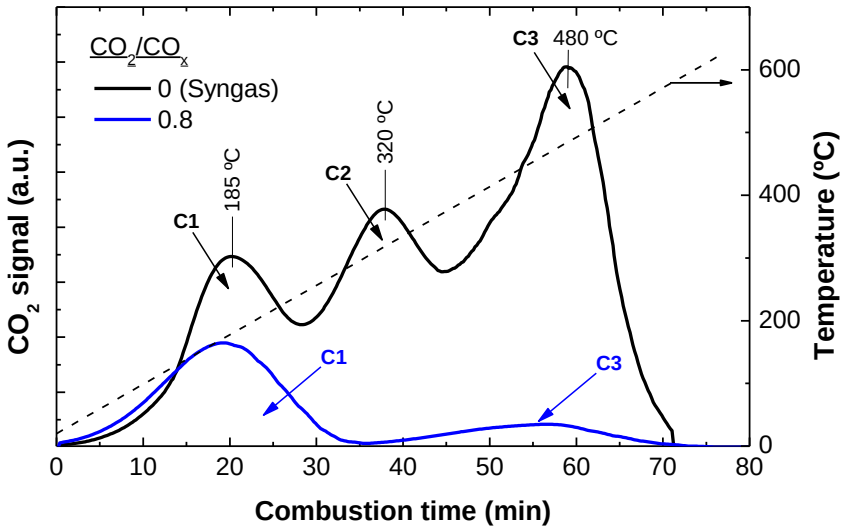

Figure 4. Comparison of TPO profiles for catalysts used in experiments with and without CO_2 in the feed. Reaction conditions: 300 ºC, 30 bar, H_2/CO_x of 3, space time 5 $g_{cat}\cdot h\cdot mol_C^{-1}$, time on stream 5 h.

Moreover, bearing in mind that CO_2 conversion is together with maximizing DME yield the main goal of the process, both targets have been studied together in Figure 5, where CO_2 conversion is defined as:

$$X_{CO_2} = \frac{F^0_{CO_2} - F_{CO_2}}{F^0_{CO_2}} \cdot 100 \qquad (32)$$

It can be observed that the objectives of maximizing CO_2 conversion and DME yield follow different trends, which hinders achieving a good compromise between both objectives, as it has already been established for conventional structure (hybrid) catalysts [61].

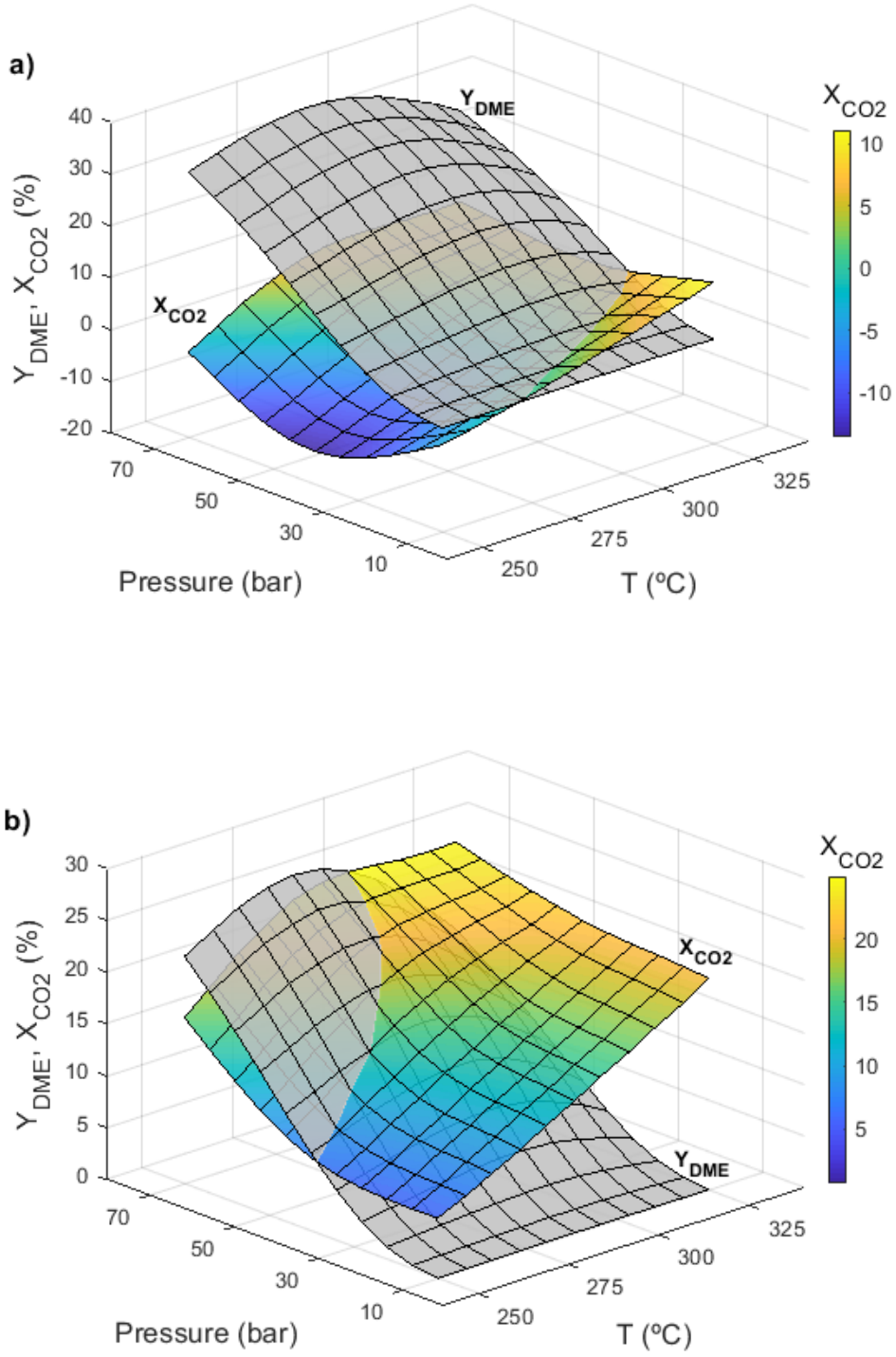

Figure 5. Evolution of DME yield and CO_2 conversion with reaction temperature and pressure for CO_2/CO_x ratios in the feed of 0.5 (a) and 0.75 (b). Reaction conditions: H_2+CO+CO_2 feed; H_2/CO_x, 3; space time, 5 $g_{cat}\cdot h\cdot mol_C^{-1}$; time on stream, 1 h.

For low CO_2 contents in the feed (Figure 5a corresponding to a 50 % of CO_2 in the fed $CO+CO_2$ mixture) the conversion of CO_2 describes a minimum at intermediate pressures, that displaces from around 30 to 50 bar when increasing reaction temperature from 250 to 325 ºC. Indeed, this Figure 5a highlights the need for determining the most suitable operating conditions, since for low temperature and intermediate pressure, not only DME yield is low, but the process may also produce CO_2, instead of achieving a net conversion of the fed CO_2. However, it is important to realize that using these core-shell structured CZZr@S-11 catalyst it is possible to settle operating conditions where both DME yield and CO_2 conversion are favored. Thus, it can be observed in Figure 5b that the most suitable operating conditions to attain a good compromise between the pursued goals (DME yield and CO_2 conversion) correspond to the highest pressure tested for temperatures in the 280-315 ºC range. Under these circumstances (say 70 bar and 305 ºC) a 23 % of both Y_{DME} and X_{CO2} is attained for CO_2/CO_x ratios of 0.75 in the feed (Figure 5b).

4. CONCLUSIONS

The CZZr@S-11 core-shell catalyst is very active for the joint hydrogenation of CO and CO_2 to DME, with a high DME selectivity and great stability. This behavior has been quantified in this work with a kinetic model that predicts the evolution of the concentration of the components in the reaction medium (DME, methanol, CO, CO_2 and hydrocarbons formed as byproducts). The relevance of considering in the kinetic model the effect of the concentrations of CO_2 and H_2O in the reaction medium, as being the cause of the attenuation of the rates of methanol synthesis and its dehydration to DME, has been proven. The model also considers the attenuation of coke deactivation by CO_2 and H_2O adsorption on the active sites.

Although the maximum DME yield and CO_2 conversion are achieved under different conditions, the kinetic model predicts that with this catalyst a good compromise between both targets is attained at 305 ºC and 70 bar and with a H_2/CO_x ratio of 3, since a value of 23 % is achieved for both targets in a single pass reaction. This objective is interesting for the development of the industrial process with this catalyst, because the environmental benefit of CO_2 valorization can be combined with the economic production of DME.

ACKNOWLEDGEMENTS

This work has been carried out with the financial support of the Ministry of Economy and Competitiveness of the Spanish Government (CTQ2016-77812-R), the Basque Government (Project IT1218-19), the ERDF funds and the European Commission (HORIZON H2020-MSCA RISE-2018. Contract No. 823745).

REFERENCES

[1] A. Rafiee, K. Rajab Khalilpour, D. Milani, M. Panahi, Trends in CO_2 conversion and utilization: A review from process systems perspective, J. Environ. Chem. Eng. 6 (2018) 5771–5794. doi:10.1016/J.JECE.2018.08.065.

[2] J. Schmidt, K. Gruber, M. Klingler, C. Klöckl, L. Ramirez Camargo, P. Regner, O. Turkovska, S. Wehrle, E. Wetterlund, A new perspective on global renewable energy systems: Why trade in energy carriers matters, Energy Environ. Sci. 12 (2019) 2022–2029. doi:10.1039/c9ee00223e.

[3] M. Raza, L. Chen, R. Ruiz, H. Chu, Influence of pentanol and dimethyl ether blending with diesel on the combustion performance and emission characteristics in a compression ignition engine under low temperature combustion mode, J. Energy Inst. 92 (2019) 1658–1669. doi:10.1016/j.joei.2019.01.008.

[4] J. Wang, Z. You, Q. Zhang, W. Deng, Synthesis of lower olefins by hydrogenation of carbon dioxide over supported iron catalysts, Catal. Today. 215 (2013) 186–193. doi:10.1016/J.CATTOD.2013.03.031.

[5] N. Djordjevic, M. Rekus, J. Vinkeloe, L. Zander, Shock tube and kinetic study on the effects of CO2 on dimethyl ether autoignition at high pressures, Energy Fuels 33 (2019) 10197-10208

[6] P. Pérez-Uriarte, A. Ateka, M. Gamero, A.T. Aguayo, J. Bilbao, Effect of the operating conditions in the transformation of DME to olefins over a HZSM-5 zeolite catalyst, Ind. Eng. Chem. Res. 55 (2016) 6569–6578. doi:10.1021/acs.iecr.6b00627.

[7] M. Fujiwara, N. Mimura, O. Sato, A. Yamaguchi, Surface modification of H-ZSM-5 with organo-disilane compound for propylene production from dimethyl ether, Microporous Mesoporous Mater. 280 (2019) 219–226.

doi:10.1016/j.micromeso.2019.02.005.

[8] J. Li, D. Jan, T. He, G. Liu, Z. Zi, Z. Wang, J. Wu, J. Wu, Nanocrystal H[Fe, Al]ZSM-5 zeolites with different silica-alumina composition for conversion of dimethyl ether to gasoline, Fuel. Process. Technol. 191 (2019) 104–110. doi: 10.1016/j.fuproc.2019.03.029.

[9] X. Su, K. Zhang, Y. Snatenkova, Z. Matieva, X. Bai, N. Kolesnichenko, W. Wu, High-efficiency nano [Zn,Al]ZSM-5 bifunctional catalysts for dimethyl ether conversion to isoparaffin-rich gasoline, Fuel Process. Technol. 198 (2020) 106242–106253. doi:10.1016/j.fuproc.2019.106242.

[10] M.C. Bauer, A. Kruse, The use of dimethyl ether as an organic extraction solvent for biomass applications in future biorefineries: A user-oriented review, Fuel. 254 (2019) 115703–115716. doi:10.1016/j.fuel.2019.115703.

[11] A. Subratti, L.J. Lalgee, N.K. Jalsa, Liquified dimethyl ether (DME): A green solvent for the extraction of hemp (Cannabis sativa L.) seed oil, Sustain. Chem. Pharm. 12 (2019) 100144–100149. doi:10.1016/j.scp.2019.100144.

[12] H. Javanmard, M. Seyyedi, S.A. Jones, S.M. Nielsen, Dimethyl Ether enhanced oil recovery in fractured reservoirs and aspects of phase behavior, Energy & Fuels. 33 (2019) 10718–10727. doi:10.1021/acs.energyfuels.9b02600.

[13] M. De Falco, M. Capocelli, G. Centi, Dimethyl ether production from CO_2 rich feedstocks in a one-step process: Thermodynamic evaluation and reactor simulation, Chem. Eng. J. 294 (2016) 400–409. doi:http://dx.doi.org/10.1016/j.cej.2016.03.009.

[14] A. Ateka, P. Pérez-Uriarte, M. Gamero, J. Ereña, A.T. Aguayo, J. Bilbao, A comparative thermodynamic study on the CO_2 conversion in the synthesis of methanol and of DME, Energy. 120 (2017) 796–804.

doi:10.1016/j.energy.2016.11.129.

[15] Z. Azizi, M. Rezaeimanesh, T. Tohidian, M.R. Rahimpour, Dimethyl ether: A review of technologies and production challenges, Chem. Eng. Process. Process Intensif. 82 (2014) 150–172. doi:http://dx.doi.org/10.1016/j.cep.2014.06.007.

[16] G. Leonzio, State of art and perspectives about the production of methanol, dimethyl ether and syngas by carbon dioxide hydrogenation, J. CO_2 Util. 27 (2018) 326–354. doi:10.1016/J.JCOU.2018.08.005.

[17] U. Mondal, G.D. Yadav, Perspective of dimethyl ether as fuel: Part I. Catalysis, J. CO_2 Util. 32 (2019) 299–320. doi:10.1016/j.jcou.2019.02.003.

[18] U. Mondal, G.D. Yadav, Perspective of dimethyl ether as fuel: Part II- analysis of reactor systems and industrial processes, 32 (2019) 321–338. doi:10.1016/j.jcou.2019.02.006.

[19] F. Moradi, M. Kazemeini, L. Vafajoo, M. Fattahi, A three dimensonal dynamic CFD simulation for the direct DME production in a fixed bed reactor, Comp. Aided Chem. Eng. 32 (2013) 247–252.

[20] F. Moradi, M. Kazemeini, M. Fattahi, A three dimensonal dynamic CFD simulation and optimization of direct DME synthesis in a fixed bed reactor, Pet. Sci. 11 (2014) 323–330.

[21] S. Papari, M. Kazemeini, M. Fattahi, Mathematical modeling of a slurry reactor for DME direct synthesis from syngas, J. Nat. Gas Chem. 21 (2012) 148-157.

[22] S. Papari, M. Kazemeini, M. Fattahi, M. Fatahi, DME direct synthesis from syngas in a large-scale three phase slurry bubble column reactor: Transient modeling, Chem. Eng. Comm. 201 (2014) 612-634.

[23] B. Khadem-Hamedani, S. Yaghmaei, M. Fattahi, S-Mashayekhan, S.M. Hosseni-Ardali, Mathematical modeling of a slurry bubble column reactor for

hydrodesulfurization of diesel fuel: Single- and two-bubble configurations, Chem. Eng. Res. Des. 100 (2015) 362-376.

[24] A. Torabi, M. Kazemeini, M. Fattahi, Developing a mathematical model for the oxidative dehydrogenation of propane in a fluidized bed reactor, Asia-Pacific J. Chem. Eng. 11 (2016) 448-459

[25] M.E.E. Abashar, Dimethyl ether synthesis in a multi-stage fluidized bed reactor, Chem. Eng. Process. Process Intensif, 122 (2017) 172-180.

[26] M.Z. Pedram, M. Kazemeini, M. Fattahi, A. Amjadian, A physicochemical evaluation of modified HZSM-5 catalyst utilized for production of dimethyl ether from methanol, Pet. Sci. Technol. 32 (2014) 904-911.

[27] F.B. Shareh, M. Kazemeini, M. Asadi, M. Fattahi, Metal promoted mordenite catalyst for methanol conversion into light olefins, Pet. Sci. Technol. 32 (2014) 1349-1356.

[28] A. García-Trenco, A. Vidal-Moya, A. Martínez, Study of the interaction between components in hybrid CuZnAl/HZSM-5 catalysts and its impact in the syngas-to-DME reaction, Catal. Today. 179 (2012) 43–51. doi:http://dx.doi.org/10.1016/j.cattod.2011.06.034.

[29] A. García-Trenco, A. Martínez, Direct synthesis of DME from syngas on hybrid CuZnAl/ZSM-5 catalysts: New insights into the role of zeolite acidity, Appl. Catal. A Gen. 411–412 (2012) 170–179. doi:http://dx.doi.org/10.1016/j.apcata.2011.10.036.

[30] G. Bonura, C. Cannilla, L. Frusteri, E. Catizzone, S. Todaro, M. Migliori, G. Giordano, F. Frusteri, Interaction effects between CuO-ZnO-ZrO_2 methanol phase and zeolite surface affecting stability of hybrid systems during one-step CO_2 hydrogenation to DME, Catal. Today. (2019). *In press.*

doi:10.1016/j.cattod.2019.08.014.

[31] E. Baktash, P. Littlewood, R. Schomäcker, A. Thomas, P.C. Stair, Alumina coated nickel nanoparticles as a highly active catalyst for dry reforming of methane, Appl. Catal. B Environ. 179 (2015) 122–127. doi:10.1016/j.apcatb.2015.05.018.

[32] P. Lakshmanan, M.S. Kim, E.D. Park, A highly loaded Ni@SiO_2 core-shell catalyst for CO methanation, Appl. Catal. A Gen. 513 (2016) 98–105. doi:10.1016/j.apcata.2015.12.038.

[33] M.A. Lucchini, A. Testino, A. Kambolis, C. Proff, C. Ludwig, Sintering and coking resistant core-shell microporous silica-nickel nanoparticles for CO methanation: Towards advanced catalysts production, Appl. Catal. B Environ. 182 (2016) 94–101. doi:10.1016/j.apcatb.2015.09.012.

[34] B. Liu, H. Xu, Z. Zhang, Platinum based core-shell catalysts for sour water-gas shift reaction, Catal. Commun. 26 (2012) 159–163. doi:10.1016/j.catcom.2012.05.013.

[35] A. Abdalla, P. Arudra, S.S. Al-Khattaf, Catalytic cracking of 1-butene to propylene using modified H-ZSM-5 catalyst: A comparative study of surface modification and core-shell synthesis, Appl. Catal. A Gen. 533 (2017) 109–120. doi:10.1016/j.apcata.2017.01.003.

[36] B. Zeng, B. Hou, L. Jia, D. Li, Y. Sun, Fischer-Tropsch synthesis over different structured catalysts: The effect of silica coating onto nanoparticles, J. Mol. Catal. A Chem. 379 (2013) 263–268. doi:10.1016/j.molcata.2013.08.008.

[37] G. Yang, N. Tsubaki, J. Shamoto, Y. Yoneyama, Y. Zhang, Confinement effect and synergistic function of H-ZSM-5/Cu-ZnO-Al_2O_3 capsule catalyst for one-step controlled synthesis, J. Am. Chem. Soc. 132 (2010) 8129–8136.

doi:10.1021/ja101882a.

[38] R. Liu, H. Tian, A. Yang, F. Zha, J. Ding, Y. Chang, Preparation of HZSM-5 membrane packed CuO–ZnO–Al_2O_3 nanoparticles for catalysing carbon dioxide hydrogenation to dimethyl ether, Appl. Surf. Sci. 345 (2015) 1–9. doi:https://doi.org/10.1016/j.apsusc.2015.03.125.

[39] Y. Sun, X. Han, Z. Zhao, Direct coating copper-zinc-aluminum oxalate with H-ZSM-5 to fabricate a highly efficient capsule-structured bifunctional catalyst for dimethyl ether production from syngas, Catal. Sci. Technol. 9 (2019) 3763–3770. doi:10.1039/c9cy00980a.

[40] R. Nie, H. Lei, S. Pan, L. Wang, J. Fei, Z. Hou, Core–shell structured CuO–ZnO@H-ZSM-5 catalysts for CO hydrogenation to dimethyl ether, Fuel. 96 (2012) 419–425. doi:http://dx.doi.org/10.1016/j.fuel.2011.12.048.

[41] G. Yang, M. Thongkam, T. Vitidsant, Y. Yoneyama, Y. Tan, N. Tsubaki, A double-shell capsule catalyst with core–shell-like structure for one-step exactly controlled synthesis of dimethyl ether from CO_2 containing syngas, Catal. Today. 171 (2011) 229–235. doi:http://dx.doi.org/10.1016/j.cattod.2011.02.021.

[42] Y. Wang, W. Wang, Y. Chen, J. Ma, R. Li, Synthesis of dimethyl ether from syngas over core–shell structure catalyst CuO–ZnO–Al_2O_3@SiO_2–Al_2O_3, Chem. Eng. J. 250 (2014) 248–256. doi:https://doi.org/10.1016/j.cej.2014.04.018.

[43] L. Tan, P. Zhang, Y. Suzuki, H. Li, L. Guo, Y. Yoneyama, J. Chen, X. Peng, N. Tsubaki, Bifunctional capsule catalyst of Al_2O_3@Cu with strengthened dehydration reaction field for direct synthesis of dimethyl ether from syngas, Ind. Eng. Chem. Res. 58 (2019) 22905–22911. doi:10.1021/acs.iecr.9b04864.

[44] M. Sánchez-Contador, A. Ateka, A.T. Aguayo, J. Bilbao, Direct synthesis of dimethyl ether from CO and CO_2 over a core-shell structured CuO-ZnO-

ZrO_2@SAPO-11 catalyst, Fuel Process. Technol. 179 (2018) 258–268. doi:https://doi.org/10.1016/j.fuproc.2018.07.009.

[45] M. Sánchez-Contador, A. Ateka, M. Ibáñez, J. Bilbao, A.T. Aguayo, Influence of the operating conditions on the behavior and deactivation of a CuO-ZnO-ZrO_2@SAPO-11 core-shell-like catalyst in the direct synthesis of DME, Renew. Energy. 138 (2019) 585–597. doi:10.1016/J.RENENE.2019.01.093.

[46] G. Natta, Catalysis, Reinhold, New York, 1955.

[47] G.H. Graaf, E.J. Stamhuis, A.A.C.M. Beenackers, Kinetics of low-pressure methanol synthesis, Chem. Eng. Sci. 43 (1988) 3185–3195. doi:https://doi.org/10.1016/0009-2509(88)85127-3.

[48] G.H. Graaf, H. Scholtens, E.J. Stamhuis, A.A.C.M. Beenackers, Intra-particle diffusion limitations in low-pressure methanol synthesis, Chem. Eng. Sci. 45 (1990) 773–783. doi:10.1016/0009-2509(90)85001-T.

[49] R.G. Herman, K. Klier, G.W. Simmons, B.P. Finn, J.B. Bulko, T.P. Kobylinski, Catalytic synthesis of methanol from CO H_2. I. Phase composition, electronic properties, and activities of the Cu/ZnO/M_2O_3 catalysts, J. Catal. 56 (1979) 407–429. doi:10.1016/0021-9517(79)90132-5.

[50] L.C. Grabow, M. Mavrikakis, Mechanism of methanol synthesis on cu through CO_2 and CO hydrogenation, ACS Catal. 1 (2011) 365–384. doi:10.1021/cs200055d.

[51] B.C. Gates, L.N. Johanson, Langmuir-Hinshelwood kinetics of the dehydration of methanol catalyzed by cation exchange resin, AIChE J. 17 (1971) 981–983. doi:10.1002/aic.690170435.

[52] C. Ortega, M. Rezaei, V. Hessel, G. Kolb, Methanol to dimethyl ether conversion over a ZSM-5 catalyst: Intrinsic kinetic study on an external recycle reactor,

Chem. Eng. J. 347 (2018) 741–753. doi:10.1016/j.cej.2018.04.160.

[53] P.O. Ibeh, F.J. García-Mateos, R. Ruiz-Rosas, J.M. Rosas, J. Rodríguez-Mirasol, T. Cordero, Acid mesoporous carbon monoliths from lignocellulosic biomass waste for methanol dehydration, Materials. 12 (2019) 2394. doi:10.3390/ma12152394.

[54] J. Palomo, M.A. Rodríguez-Cano, J. Rodríguez-Mirasol, T. Cordero, On the kinetics of methanol dehydration to dimethyl ether on Zr-loaded P-containing mesoporous activated carbon catalyst, Chem. Eng. J. 378 (2019) 122198–122207. doi:10.1016/j.cej.2019.122198.

[55] C. V. Ovesen, P. Stoltze, J.K. Nørskov, C.T. Campbell, A kinetic model of the water gas shift reaction, J. Catal. 134 (1992) 445–468. doi:10.1016/0021-9517(92)90334-E.

[56] C. Rhodes, G.J. Hutchings, A.M. Ward, Water-gas shift reaction: finding the mechanistic boundary, Catal. Today. 23 (1995) 43–58. doi:https://doi.org/10.1016/0920-5861(94)00135-O.

[57] D. Ma, C.R.F. Lund, Assessing high-temperature water-gas shift membrane reactors, Ind. Eng. Chem. Res. 42 (2003) 711–717. https://www.scopus.com/inward/record.uri?eid=2-s2.0-0037453781&partnerID=40&md5=043d971824a854e31239b2d6d3bcc692.

[58] A.R. De La Osa, A. De Lucas, A. Romero, J.L. Valverde, P. Sánchez, Kinetic models discrimination for the high pressure WGS reaction over a commercial CoMo catalyst, Int. J. Hydrogen Energy. 36 (2011) 9673–9684. doi:10.1016/j.ijhydene.2011.05.043.

[59] R. Burch, A. Goguet, F.C. Meunier, A critical analysis of the experimental evidence for and against a formate mechanism for high activity water-gas shift

catalysts, Appl. Catal. A Gen. 409–410 (2011) 3–12. doi:10.1016/j.apcata.2011.09.034.

[60] J. Ereña, I. Sierra, A.T. Aguayo, A. Ateka, M. Olazar, J. Bilbao, Kinetic modelling of dimethyl ether synthesis from (H_2+CO_2) by considering catalyst deactivation, Chem. Eng. J. 174 (2011) 660–667. doi:10.1016/j.cej.2011.09.067.

[61] A. Ateka, J. Ereña, J. Bilbao, A.T. Aguayo, Kinetic modeling of the direct synthesis of dimethyl ether over a CuO-ZnO-MnO/SAPO-18 catalyst and assessment of the CO_2 conversion, Fuel Process. Technol. 181 (2018) 233–243. doi:10.1016/j.fuproc.2018.09.024.

[62] M. Sánchez-Contador, A. Ateka, P. Rodriguez-Vega, J. Bilbao, A.T. Aguayo, Optimization of the Zr content in the CuO-ZnO-ZrO_2/SAPO-11 catalyst for the selective hydrogenation of CO+CO_2 mixtures in the direct synthesis of dimethyl ether, Ind. Eng. Chem. Res. 57 (2018) 1169–1178. doi:10.1021/acs.iecr.7b04345.

[63] M. Sánchez-Contador, A. Ateka, A.T. Aguayo, J. Bilbao, Behavior of SAPO-11 as acid function in the direct synthesis of dimethyl ether from syngas and CO_2, J. Ind. Eng. Chem. 63 (2018) 245–254. doi:10.1016/j.jiec.2018.02.022.

[64] G. Yang, C. Xing, W. Hirohama, Y. Jin, C. Zeng, Y. Suehiro, T. Wang, Y. Yoneyama, N. Tsubaki, Tandem catalytic synthesis of light isoparaffin from syngas via Fischer–Tropsch synthesis by newly developed core–shell-like zeolite capsule catalysts, Catal. Today. 215 (2013) 29–35. doi:https://doi.org/10.1016/j.cattod.2013.01.010.

[65] K. Pinkaew, G. Yang, T. Vitidsant, Y. Jin, C. Zeng, Y. Yoneyama, N. Tsubaki, A new core–shell-like capsule catalyst with SAPO-46 zeolite shell encapsulated Cr/ZnO for the controlled tandem synthesis of dimethyl ether from syngas, Fuel. 111 (2013) 727–732. doi:http://dx.doi.org/10.1016/j.fuel.2013.03.027.

[66] R. Phienluphon, K. Pinkaew, G. Yang, J. Li, Q. Wei, Y. Yoneyama, T. Vitidsant, N. Tsubaki, Designing core ($Cu/ZnO/Al_2O_3$)–shell (SAPO-11) zeolite capsule catalyst with a facile physical way for dimethyl ether direct synthesis from syngas, Chem. Eng. J. 270 (2015) 605–611. doi:https://doi.org/10.1016/j.cej.2015.02.071.

[67] A.G. Gayubo, J. Vicente, J. Ereña, L. Oar-Arteta, M.J. Azkoiti, M. Olazar, J. Bilbao, Causes of deactivation of bifunctional catalysts made up of CuO-ZnO-Al_2O_3 and desilicated HZSM-5 zeolite in DME steam reforming, Appl. Catal. A Gen. 483 (2014) 76–84. doi:10.1016/j.apcata.2014.06.031.

[68] A. Ateka, J. Ereña, M. Sánchez-Contador, P. Perez-Uriarte, J. Bilbao, A.T. Aguayo, Capability of the direct dimethyl ether synthesis process for the conversion of carbon dioxide, Appl. Sci. 8 (2018) 677–690. doi:10.3390/app8050677.

[69] M. Fattahi, M. Kazemeini, F. Khorasheh, A. Rashidi, Kinetic modeling of oxidative dehydrogenation of propane (ODHP) over a vanadium-graphene catalyst: Application of the DOE and ANN methodologies, J. Ind. Eng. Chem. 20 (2014) 2236–2247.

[70] K. Toch, J.W. Thybaut, G.B. Marin, A systematic methodology for kinetic modeling of chemical reactions applied to n-hexane hydroisomerization, AIChE J. 61 (2015) 880–892. doi:10.1002/aic.14680.

[71] T. Cordero-Lanzac, A.T. Aguayo, A.G. Gayubo, P. Castaño, J. Bilbao, Simultaneous modeling of the kinetics for n-pentane cracking and the deactivation of a HZSM-5 based catalyst, Chem. Eng. J. 331 (2018) 818–830. doi:10.1016/j.cej.2017.08.106.

[72] A.G. Gayubo, A.T. Aguayo, A.L. Morán, M. Olazar, J. Bilbao, Role of water in

the kinetic modeling of catalyst deactivation in the MTG process, AIChE J. 48 (2002) 1561–1571. doi:10.1002/aic.690480718.

[73] A.G. Gayubo, A.T. Aguayo, A.E. Sánchez Del Campo, A.M. Tarrío, J. Bilbao, Kinetic modeling of methanol transformation into olefins on a SAPO-34 catalyst, Ind. Eng. Chem. Res. 39 (2000) 292–300. doi:10.1021/ie990188z.

[74] G. Bonura, M. Migliori, L. Frusteri, C. Cannilla, E. Catizzone, G. Giordano, F. Frusteri, Acidity control of zeolite functionality on activity and stability of hybrid catalysts during DME production via CO_2 hydrogenation, J. CO2 Util. 24 (2018) 398–406. doi:10.1016/j.jcou.2018.01.028.

[75] S. Ren, W.R. Shoemaker, X. Wang, Z. Shang, N. Klinghoffer, S. Li, M. Yu, X. He, T.A. White, X. Liang, Highly active and selective Cu-ZnO based catalyst for methanol and dimethyl ether synthesis via CO_2 hydrogenation, Fuel. 239 (2019) 1125–1133. doi:10.1016/J.FUEL.2018.11.105.

[76] T. Cordero-Lanzac, A. Ateka, P. Pérez-Uriarte, P. Castaño, A.T. Aguayo, J. Bilbao, Insight into the deactivation and regeneration of HZSM-5 zeolite catalysts in the conversion of dimethyl ether to olefins, Ind. Eng. Chem. Res. 57 (2018) 13689–13702. doi:10.1021/acs.iecr.8b03308.

[77] I. Sierra, J. Ereña, A.T. Aguayo, M. Olazar, J. Bilbao, Deactivation kinetics for direct dimethyl ether synthesis on a CuO-ZnO-Al_2O_3/γ-Al_2O_3 Catalyst, Ind. Eng. Chem. Res. 49 (2010) 481–489. doi:10.1021/ie900978a.

[78] Z-Z. Qin, T.M. Su, H-B. Ji, Y-X, Jiang, R-W. Liu, J-H. Chen, Experimental and theoretical study of the intrinsic kinetics for dimethyl ether synthesis from CO_2 over Cu–Fe–Zr/HZSM-5, AIChE J. 61 (2015) 1613-1627. doi 10.1002/aic.14743

[79] M. Bjørgen, S. Svelle, F. Joensen, J. Nerlov, S. Kolboe, F. Bonino, L. Palumbo, S. Bordiga, U. Olsbye, Conversion of methanol to hydrocarbons over zeolite H-

ZSM-5: On the origin of the olefinic species, J. Catal. 249 (2007) 195–207. doi:10.1016/j.jcat.2007.04.006.

[80] B. Barghi, M. Fattahi, F. Khorasheh, The modeling of kinetics and catalyst deactivation in propane dehydrogenation over Pt-Sn/γ-Al_2O_3 in presence of water as an oxygenated additive, Pet. Sci. Technol. 32 (2014) 1139-1149

[81] Ibarra, E. Rodriguez, U. Sedran, J.M. Arandes, J. Bilbao, Synergy in the cracking of a blend of bio-oil and vacuum gasoil under fluid catalytic cracking conditions, Ind. Eng. Chem. Res. 55 (2016) 1872-1880.

Supporting information for:

Kinetic modeling of CO_2 + CO hydrogenation to DME over a CuO-ZnO-ZrO_2@SAPO-11 core-shell catalyst

Ainara Ateka*, Miguel Sánchez-Contador, Ander Portillo, Javier Bilbao, Andres T. Aguayo

Department of Chemical Engineering, University of the Basque Country UPV/EHU, P.O. Box 644, 48080 Bilbao, Spain

*Corresponding author. *Tel.:* 34-94-6015361. *E-mail address*: ainara.ateka@ehu.eus

S. 1. Methodology for determining the kinetic parameters and for assessing the significance and validity of the models

The kinetic parameters to be calculated are the kinetic constants of each j reaction, k_j, related to the temperature by means of the reparameterized Arrhenius equation (Eq. S1), for reducing the correlation between the pre-exponential factor and the activation energy [1-4].

$$k_j = A_{0,i} \exp\left(-\frac{E_j}{RT}\right) = k_j^* \exp\left[-\frac{E_j}{R}\left(\frac{1}{T}-\frac{1}{T^*}\right)\right] \quad \text{(S1)}$$

Thus, k_j^* (kinetic constant at reference temperature T* (275 ºC)) and E_j (activation energy) are the parameters to be optimized. Likewise, the equilibrium constants have also been reparameterized (Eq. (S2), and the parameters to be optimized are here $K_{ads,i}^*$ (the adsorption constant at reference temperature) and $\Delta H_{ads,i}^0$ (the corresponding adsorption energy):

$$K_{ads,i} = K_{ads,i}^* \exp\left[\frac{\Delta H_{ads,i}^0}{R}\left(\frac{1}{T}-\frac{1}{T^*}\right)\right] \quad \text{(S2)}$$

For the calculation of these parameters of the model best fitting the experimental results, a calculation program has been developed in MATLAB for the multivariable non linear regression, as to minimize the defined Objective Function (O.F., Eq. (S3)). This O.F. is composed of two terms, the first is related to the error of the lack of fit at zero time on stream and the second to the lack of fit of the deactivation kinetics:

$$\begin{aligned} \text{O.F.} &= \text{error}_0 + \text{error}_d = \sum_{i=1}^{n_l} \omega_i \left(\phi_{i,0} + \phi_{i,d}\right) = \\ &= \sum_{i=1}^{n_l}\left(\frac{1}{\overline{X_l}}\right)\left[\left(\sum_{j=1}^{p} R_j \left(\left(\overline{y}_{i,j}^*\right)_0 - \left(y_{i,j}\right)_0\right)^2 / p\right) + \left(\sum_{j=1}^{p} R_j \left(\left(\overline{y}_{i,j}^*\right)_d - \left(y_{i,j}\right)_d\right)^2 / p\right)\right] \end{aligned} \quad \text{(S3)}$$

where ω_i represent the weight factor assigned to each component *i*; $\phi_{i,0}$ the total sum of squares for each component *i* at j experimental condition at zero time on stream, whereas $\phi_{i,d}$ is that with time; $\bar{y}^*_{i,j}$ is the average experimental value of the concentration of component *i*, determined in repeated runs at the same *j* conditions; while $y_{i,j}$ the calculated concentration for component *i*; n_l is the number of components involved in the kinetic scheme and; p, the total number of experiments carried out.

The calculation program, after collecting data on the operating conditions (temperature, pressure, space-time, molar fraction and flowrate at the reactor entrance, and the experimental values of components concentration at the reactor outlet at different reaction times), uses simultaneously a subroutine for determining the individual and global errors of the lack of fit according to Eq. (S3); a function for determining the composition and activity values; and a derivative function to solve the differential equation system (kinetic equations) considered in each model, and proceeds to minimize the O.F. (Eq. (S3)), giving as a result the kinetic parameters of best fit, and the confidence intervals.

For assessing the significance and validity of the models, a statistic study based on the Fischer exact test has been carried out, and the fittings obtained with the different models have been compared as to determine whether the fitting obtained with the more complex model over the more simple model is significant. In brief, the sum of square errors used for the study can be described as shown in Eq. (S4), and the expressions in Eqs. (S5) and (S6) have been used to determine the significance of the models individually (comparing the lack of fit with the experimental error) and for comparing the models by pairs, respectively, and assessing whether the improvement obtained with

model B (more complex) is significant over the fitting obtained with model A (simple). The procedure has been explained more in detail elsewhere [3,4].

$$SSE = \sum_{i=1}^{n_l} \sum_{j=1}^{p} \left(\bar{y}^{*}_{i,j} - y_{i,j} \right)^2 \tag{S4}$$

$$F_S = \frac{s_a^2}{s_{exp.}^2} < F_{1-\alpha}(\upsilon_a, \upsilon_{exp}) \text{ for a confidence interval of 95 \% } (\alpha=0.05) \tag{S5}$$

$$F_{a-b} = \frac{(SSE_a - SSE_b)/SSE_b}{(\upsilon_a - \upsilon_b)/\upsilon_b} > F_{1-\alpha}((\upsilon_a - \upsilon_b)/, \upsilon_b) \quad \text{for} \quad \upsilon_a > \upsilon_b \quad \text{and} \quad SSE_a > SSE_b$$

$$\text{while } F_{a-b} = \frac{SSE_a/\upsilon_a}{SSE_b/\upsilon_b} = \frac{s_a^2}{s_b^2} > F_{1-\alpha}(\upsilon_a, \upsilon_b) \text{ when } \upsilon_a = \upsilon_b \text{ and } s_a^2 > s_b^2 \tag{S6}$$

S. 2. Fitting of the selected model to the experimental results at various reaction conditions

The comparison of the fitting obtained with models 1, 2, 4A and 5B to the experimental values of oxygenates (DME and methanol) yields for different values of space time is depicted in Figure S1, while Figure S2 shows the fitting of all the components in the reaction medium obtained with each model.

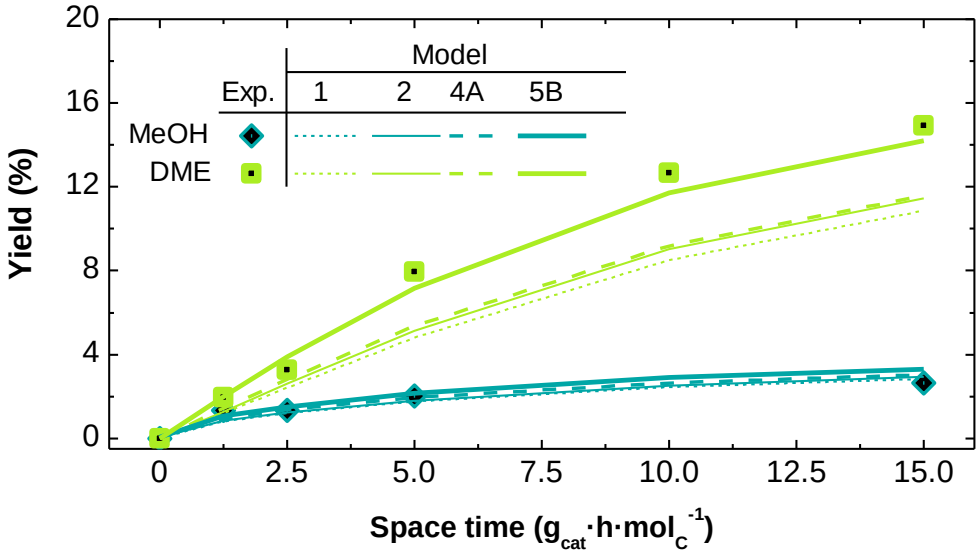

Figure S1. Comparison of the fitting improvement obtained with model 5B over models 4A, 2 and 1, for oxygenates yields (MeOH and DME). Reaction conditions: 300 ºC, 30 bar, CO_2/CO_x= 0.5, H_2/CO_x= 3.

The following Figures S2-S6 show the fitting quality of the selected model (5B) to the experimental results at different operating conditions.

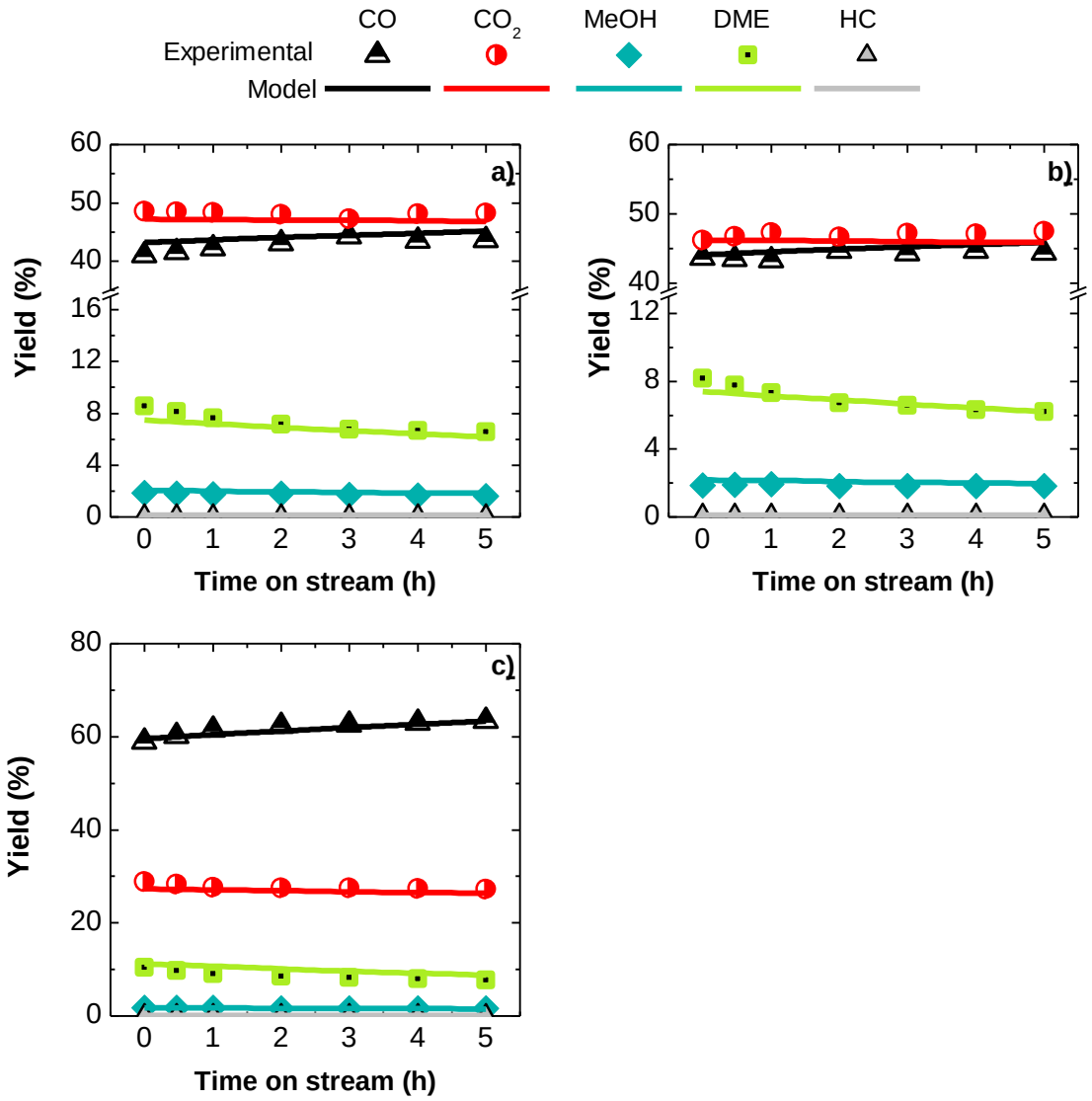

Figure S2. Fitting of the model to the experimental values of CO, CO_2, MeOH, DME and HC yields evolution with time on stream for different H_2/CO_x ratios in the feed: 2.5 (a), 3 (b) and 4 (c). Reaction conditions: 300 ºC, 30 bar, CO_2/CO_x= 0.5, space time 5 $g_{cat}\cdot h\cdot mol_C^{-1}$.

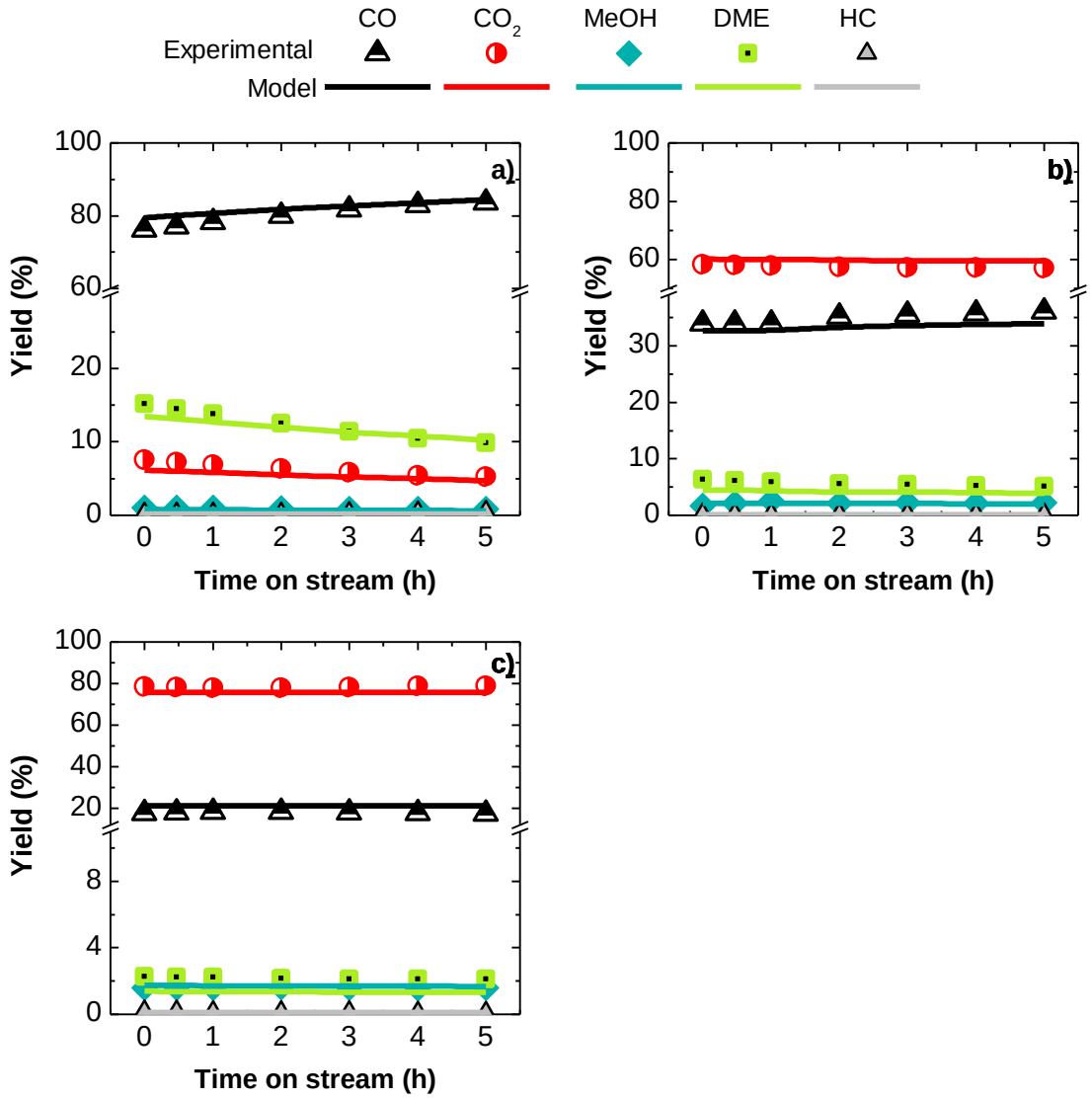

Figure S3. Fitting of the model to the experimental values of CO, CO_2, MeOH, DME and HC yields evolution with time on stream for different CO_2/CO_x ratios in the feed: 0 (a), 0.75 (b) and 1 (c). Reaction conditions: 300 ºC, 30 bar, H_2/CO_x= 3, space time 5 $g_{cat}\cdot h\cdot mol_C^{-1}$.

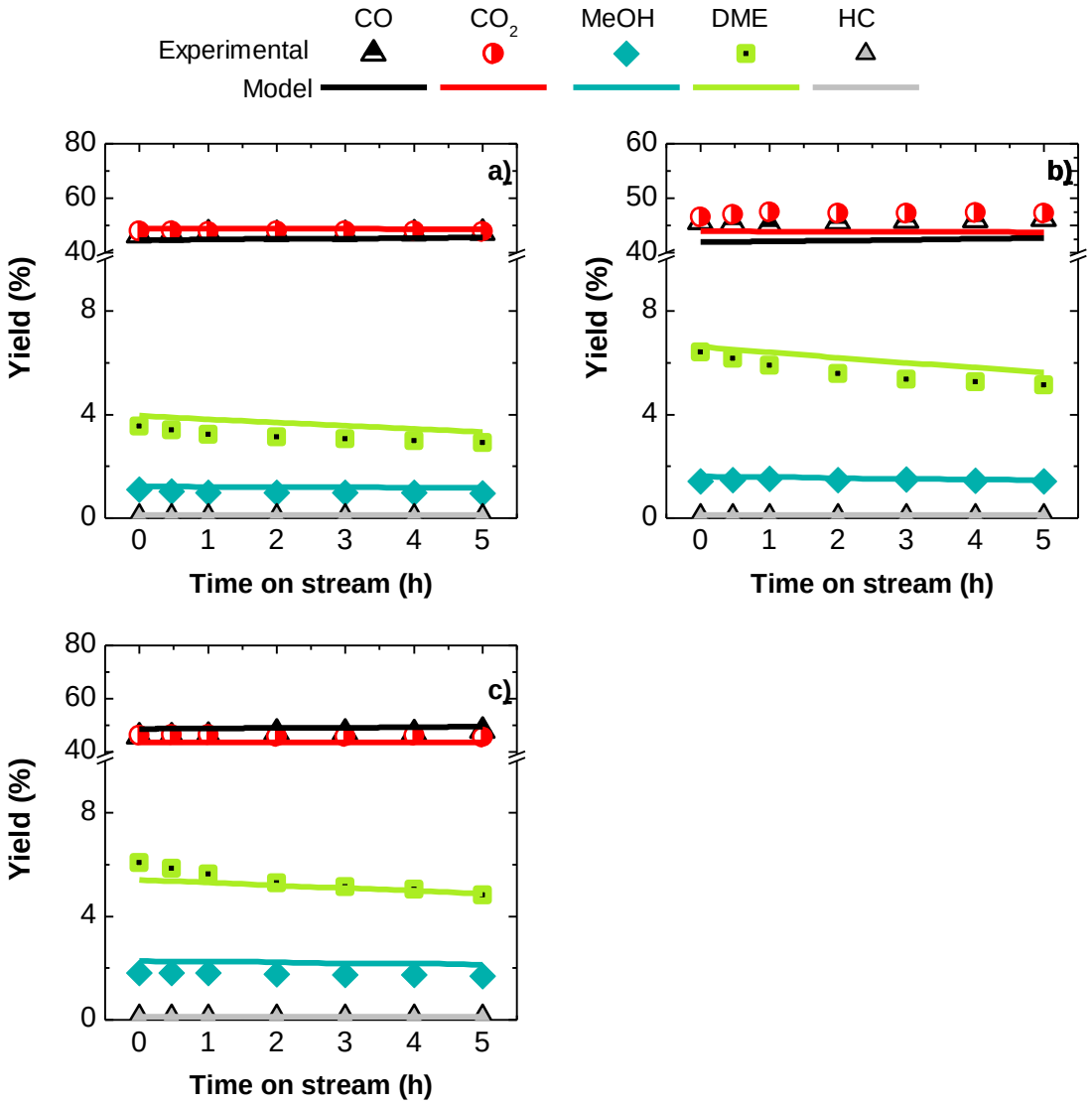

Figure S4. Fitting of the model to the experimental values of CO, CO_2, MeOH, DME and HC yields evolution with time on stream for different reaction temperatures: 250 ºC (a), 275 ºC (b) and 325 ºC (c). Reaction conditions: 30 bar, H_2/CO_x= 3, CO_2/CO_x= 0.5, space time 5 $g_{cat}\cdot h\cdot mol_C^{-1}$.

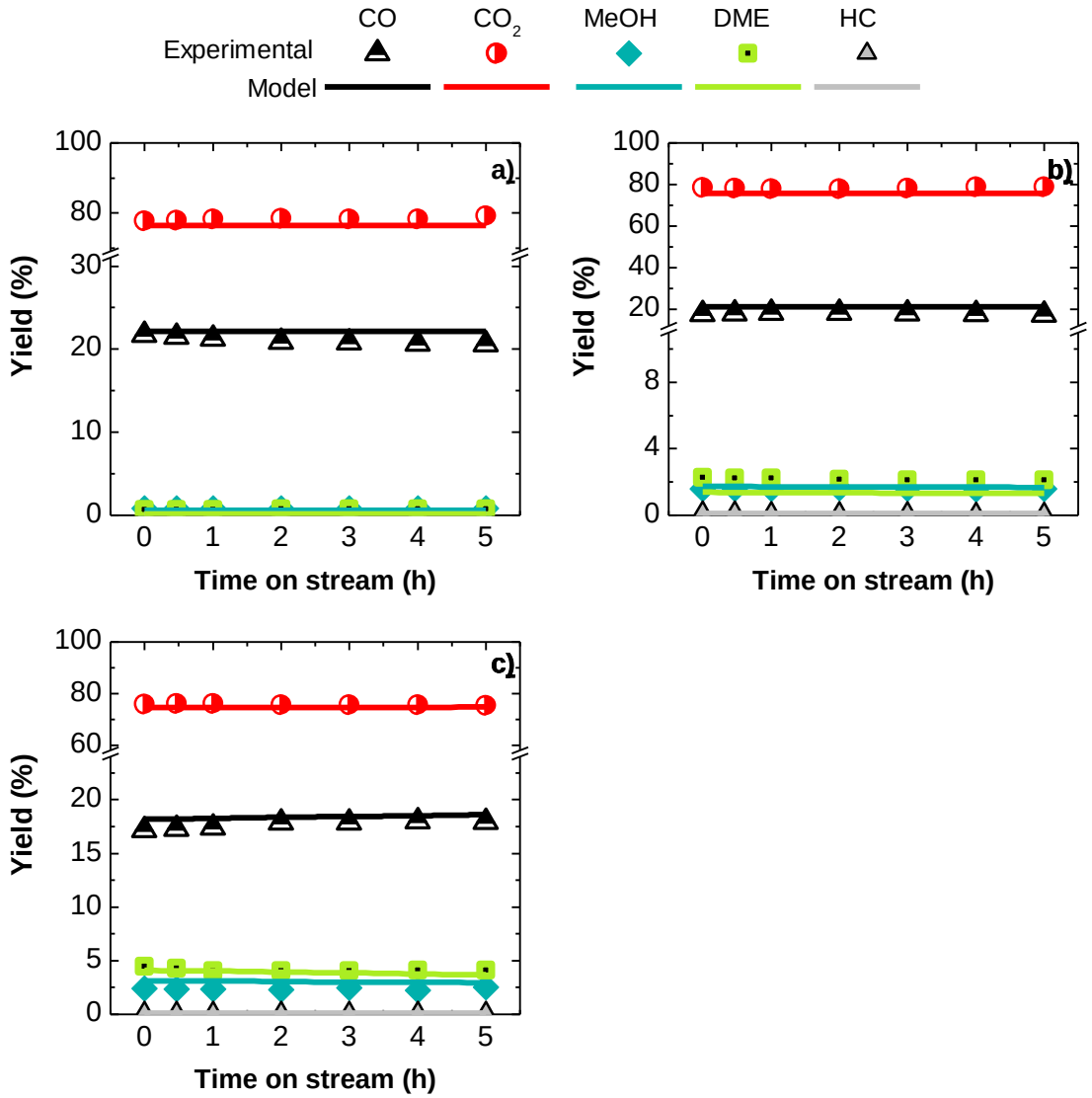

Figure S5. Fitting of the model to the experimental values of CO, CO_2, MeOH, DME and HC yields evolution with time on stream for different reaction pressures: 20 bar (a), 30 bar (b) and 40 bar (c). Reaction conditions: 300 ºC, H_2/CO_x= 3, CO_2/CO_x= 1, space time 5 $g_{cat}\cdot h\cdot mol_C^{-1}$.

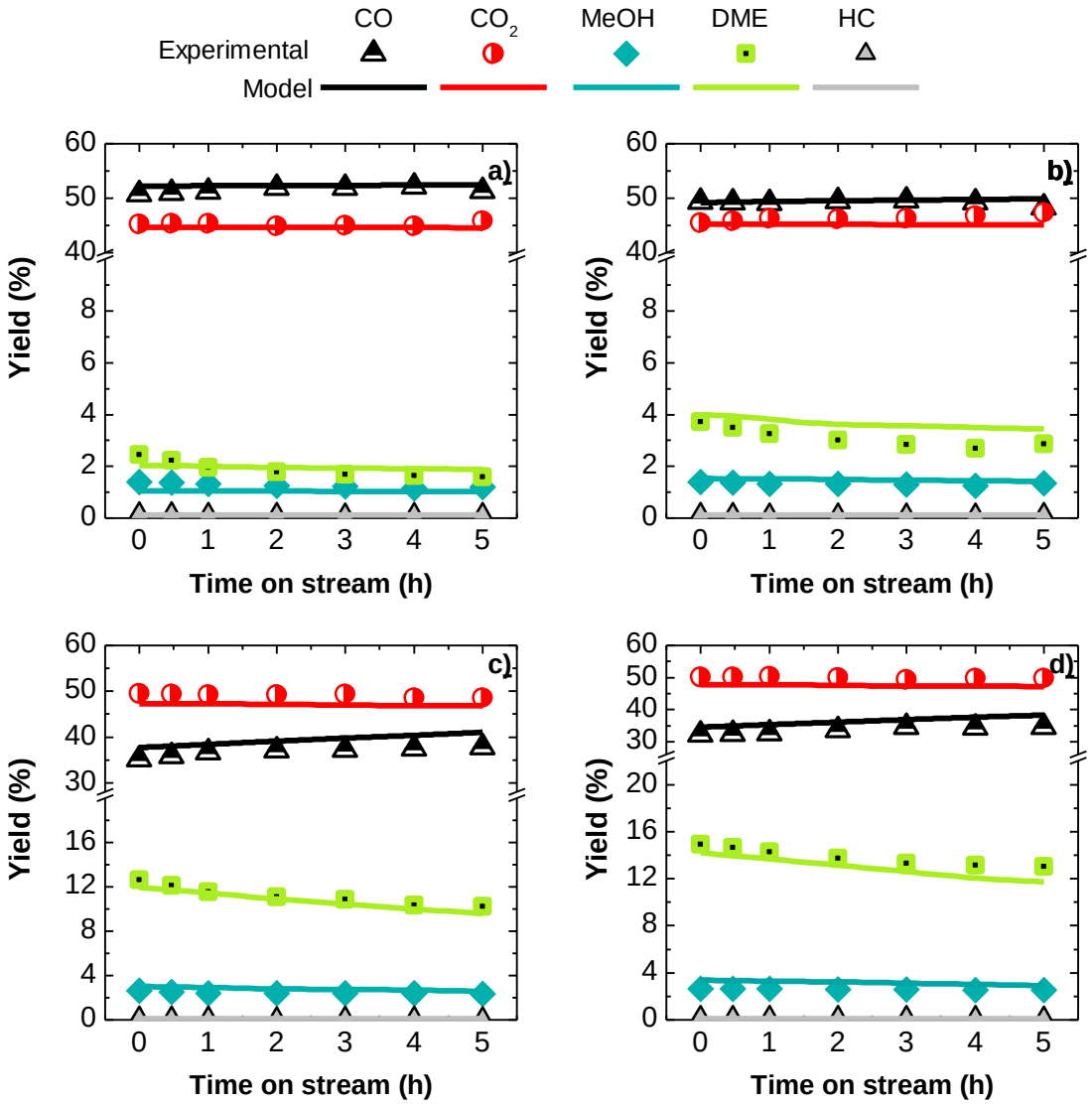

Figure S6. Fitting of the model to the experimental values of CO, CO_2, MeOH, DME and HC yields evolution with time on stream for different space time values: 1.25 (a), 2.5 (b), 10 (c) and 15 (d). Reaction conditions: 300 ºC, 30 bar, H_2/CO_x= 3, CO_2/CO_x= 0.5.

References

[1] A.K. Agarwal, M.L. Brisk, Sequential Experimental Design for Precise Parameter Estimation. 1. Use of Reparameterization, Ind. Eng. Chem. Process Des. Dev. 24 (1985) 203–207. doi:10.1021/i200028a034.

[2] A.G. Gayubo, A.T. Aguayo, A.E. Sánchez Del Campo, A.M. Tarrío, J. Bilbao, Kinetic modeling of methanol transformation into olefins on a SAPO-34 catalyst, Ind. Eng. Chem. Res. 39 (2000) 292–300. doi:10.1021/ie990188z.

[3] P. Pérez-Uriarte, A. Ateka, A.T. Aguayo, A.G. Gayubo, J. Bilbao, Kinetic model for the reaction of DME to olefins over a HZSM-5 zeolite catalyst, Chem. Eng. J. 302 (2016). doi:10.1016/j.cej.2016.05.096.

[4] A. Ateka, J. Ereña, J. Bilbao, A.T. Aguayo, Kinetic modeling of the direct synthesis of dimethyl ether over a CuO-ZnO-MnO/SAPO-18 catalyst and assessment of the CO_2 conversion, Fuel Process. Technol. 181 (2018) 233–243. doi:10.1016/j.fuproc.2018.09.024.